Product rotational polarization in photoninitiated bimolecular reactions

F. J. Aoiz, M. Brouard, and P. A. Enriquez

Citation: The Journal of Chemical Physics **105**, 4964 (1996); doi: 10.1063/1.472346
View online: http://dx.doi.org/10.1063/1.472346
View Table of Contents: http://scitation.aip.org/content/aip/journal/jcp/105/12?ver=pdfcov
Published by the AIP Publishing

Product rotational polarization in photon-initiated bimolecular reactions

F. J. Aoiz
Departamento de Quimica Fisica I, Facultad de Ciencias Quimicas, Universidad Complutense, 28040 Madrid, Spain

M. Brouard
Physical and Theoretical Chemistry Laboratory, South Parks Road, Oxford, OX1 3QZ, United Kingdom

P. A. Enriquez
Departamento de Quimica, Universidad de La Rioja, Obispo Bustamante, 3, 26001 Logrono, La Rioja, Spain

(Received 26 April 1996; accepted 7 June 1996)

This paper concerns the semiclassical description, calculation and measurement of angular momentum polarization in the products of elementary gas-phase bimolecular reactions. A unified, semiclassical treatment of the centre-of-mass correlated ($\mathbf{k},\mathbf{k}',\mathbf{j}'$) angular distribution involving the reagent and product relative velocity and the product angular momentum vectors is described, and is related to other methodologies already existing in the literature. Explicit expressions are provided enabling experimentalists to extract rotational polarization information from crossed-molecular beam and photon-initiated reaction studies, under a variety of experimental conditions. Furthermore, the strategy developed is well suited to the theoretical calculation of reaction product polarization, in particular, using classical trajectory methods. An illustrative example of such a calculation is presented, and the centre-of-mass polarization data provided is used to simulate the laboratory frame rotational moments that can be determined experimentally using 1+1 Doppler-resolved polarized Laser product probing techniques. © *1996 American Institute of Physics.* [S0021-9606(96)04134-7]

I. INTRODUCTION

Since the pioneering work of Fano and Macek[1] and of Herschbach and co-workers,[2–4] it has been recognized that a detailed, three-dimensional picture of the dynamics of reactive collisions emerges with the determination of the correlated angular distribution describing the mutual orientations of the reagent and product linear and angular momenta. Herschbach and co-workers identified a hierarchy of ''vector correlations,'' the most familiar being that between the vectors $\mathbf{k}$ and $\mathbf{k}'$ (the reagent and product relative velocity vectors) characterized by the differential cross-section $d\sigma/d\omega_t$.[5] In the context of the present work, which concerns reactions involving rotationally *un*polarization reagent molecules, the vectors of interest are $\mathbf{k}$, $\mathbf{k}'$, and $\mathbf{j}'$ (the product rotational angular momentum): The angular distribution describing the relative orientation of these vectors in space may be termed the $\mathbf{k}-\mathbf{k}'-\mathbf{j}'$ distribution and the correlations which characterize it, double and triple vector correlations.

Renewed interest in measuring features of the $\mathbf{k}-\mathbf{k}'-\mathbf{j}'$ distribution has been awakened with the development of Doppler-resolved or time-of-flight strategies for probing the *product state selective* dynamics of photon-initiated bimolecular reactions (for leading references see Refs. 6–8). The polarized laser pump–probe strategy has been successfully exploited by a number of groups to determine product state-selective differential cross-sections with high precision. Measurements have been performed either under thermal (''bulb'') conditions[9,10] or, with potentially higher collision energy and angular resolution, under jet cooled expansion conditions.[6,7,11] The enhanced reagent number densities achieved using these techniques, compared with those typically obtained in conventional crossed-molecular beam methods, have now enabled full state-to-state differential cross-sections to be measured for the $Cl+CH_4$ reaction.[12–15]

The use of polarized lasers for both initiation and probing stages of the photon-initiated reaction sequence also provides a means of probing product state-resolved rotational polarization, in principle as a function of centre-of-mass (CM) scattering angle. Indeed, a number of studies have now yielded product state selective rotational alignments[7,8,10,16–18] although, to date, few have provided quantitative insight into their dependence on centre-of-mass (CM) scattering angle.[18] Such studies rely on the ability to transform laboratory (LAB) frame measurements to the CM quantities of interest, and a number of formalisms have been developed to facilitate this.[19–21] That suggested by Aoiz *et al.*[19] and employed by Brouard and Simons[8] and by Hall[10] and their co-workers, and often used by practitioners of Doppler-resolved laser induced fluorescence (LIF) product probing methods, is based on the semiclassical bipolar moment expansion formalism proposed originally by Dixon[22] in the context of measurement of fragment vector correlations in molecular photodissociation (the primary process in the photon-initiated reaction sequence). An alternative, powerful procedure, developed recently by Shafer-Ray *et al.*,[20,21] and closely related to the procedures developed by Zare and Orr-Ewing,[7] employs a spherical harmonic expansion of the CM angular momentum distribution in terms of polarization dependent ''generalized'' differential cross-sections (PDDCS). The latter can be related readily to the quantum mechanical multi-

 0021-9606/96/105(12)/4964/19/$10.00

pole moments of the angular momentum distribution, obtainable from quantum scattering calculations, but also provide a transparent link between measured LAB frame quantities and the CM properties of interest.

The purpose of this paper is:

(a) provide a unified description of the CM $\mathbf{k}$–$\mathbf{k}'$–j′ distribution and thus a link between the various alternative descriptions which already exist in the literature (Section II);

(b) provide detailed working equations enabling experimentalists to extract information about the $\mathbf{k}$–$\mathbf{k}'$–$\mathbf{j}'$ distribution using Doppler resolved product probing techniques, either from crossed-beam experiments or from studies of photon-initiated bimolecular reactions (Section III);

(c) illustrate, via quasi-classical trajectory calculation and numerical simulation,

(i) the nature of the CM scattering angle dependent rotational polarization data being sought (Sec. IV A), and

(ii) the type of LAB frame information which may be obtained from Doppler-resolved product probing of reaction products, under room temperature ''bulb'' conditions (Sec. IV B).

The current work is restricted to the state-resolved probing of the diatomic AB fragments of a triatomic A+BC reaction. The more general treatment required to study reactions involving partner products, C, which have internal energy level structure (e.g., those involving polyatomic reagents), and applications of the derived machinery to experimental systems, will be presented elsewhere.[18,23]

II. THE CENTRE-OF-MASS k–k′–j′ ANGULAR DISTRIBUTION

For an atom-diatom reaction, the CM $\mathbf{k}$–$\mathbf{k}'$–$\mathbf{j}'$ semiclassical probability density function for a given product state, constrained to a single CM speed by energy conservation, can be written

$$P(\omega_t,\omega_r,w)=\delta(w-w_i)P(\omega_t,\omega_r)=\frac{1}{\sigma}\frac{d^2\sigma}{d\omega_t d\omega_r}\,\delta(w-w_i), \tag{1}$$

where w is the CM frame speed of the product and w_i its value for a state i at a given total energy. The angles $\omega_t=\theta_t,\phi_t$ and $\omega_r=\theta_r,\phi_r$ refer to the coordinates of the unit vectors $\hat{\mathbf{k}}'$ and $\hat{\mathbf{j}}'$ along the directions of the product relative velocity and rotational angular momentum vectors, respectively, in a frame (the CM frame) whose z-axis lies in the direction of the *reagent* relative velocity, $\mathbf{k}$. We define the reagent and product relative velocities in terms of the reagent and product CM velocities as $\mathbf{k}=\mathbf{v}_A-\mathbf{v}_{BC}$ and $\mathbf{k}'=\mathbf{v}_{AB}-\mathbf{v}_C$. As mentioned above, the more general case in which $P(\omega_q,\omega_r,w)$ is non-separable, appropriate for reactions involving polyatomic species, will be examined elsewhere.[23]

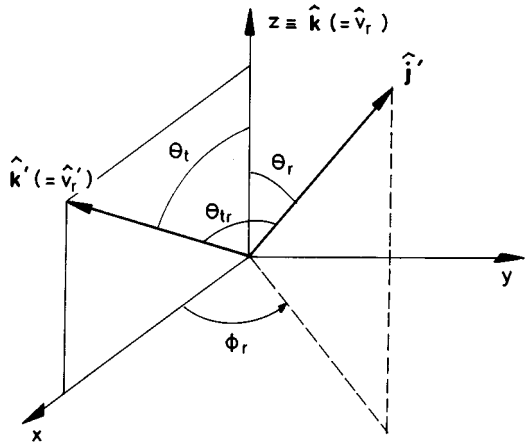

FIG. 1. The CM coordinate system used to characterize the $\mathbf{k},\mathbf{k}',\mathbf{j}'$ distribution, as described in Sec. II.

The semiclassical angular distribution can be expanded in terms of bipolar harmonics[22]

$$P(\omega_t,\omega_r)=\frac{1}{16\pi^2}\sum_{KQ}\sum_{k_1k_2}[k_1]\times[k_2]h_Q^K(k_1,k_2)B_Q^K(k_1,k_2;\omega_t,\omega_r), \tag{2}$$

where $[n]\equiv(2n+1)$ and the bipolar harmonics, defined as Dixon,[22] Brink and Satchler,[24] and Zare,[25] are given by

$$B_Q^K(k_1,k_2;\omega_t,\omega_r)=\sum_{q_1q_2}(-1)^{K-Q}[K]^{1/2}\begin{pmatrix}k_1 & K & k_2\\ q_1 & -Q & q_2\end{pmatrix}\times C_{k_1q_1}(\theta_t,\phi_t)C_{k_2q_2}(\theta_r,\phi_r). \tag{3}$$

The expectation values of the bipolar harmonics, the CM *bipolar moments*, which characterize the $\mathbf{k}$–$\mathbf{k}'$–$\mathbf{j}'$ triple vector correlation, are defined

$$h_Q^K(k_1,k_2)=\int B_Q^K(k_1,k_2;\omega_t,\omega_r)^*\times P(\omega_t,\omega_r)d(\cos\theta_t)d(\cos\theta_r)d\phi_t\,d\phi_r. \tag{4}$$

Since we define the CM xz plane as that containing $\hat{\mathbf{k}}'$ (i.e., $\phi_t=0$, see Fig. 1), it is readily shown that for $P(\omega_t,\omega_r)$ to be real, Q must equal zero. Therefore, the expression for the angular distribution becomes

$$P(\omega_t,\omega_r)=\frac{1}{16\pi^2}\sum_{K}\sum_{k_1k_2}[k_1]\times[k_2]h_0^K(k_1,k_2)B_0^K(k_1,k_2;\omega_t,\omega_r) \tag{5}$$

and, in addition, the bipolar moments must satisfy the relation

$$h_0^K(k_1,k_2)=(-1)^{K+k_1+k_2}h_0^K(k_1,k_2)^*. \tag{6}$$

Equation (6) implies that if $K+k_2+k_2$ is even, $h_0^K(k_1,k_2)$ is real, and pure imaginary otherwise. The above expansion

[Eq. (5)] is equivalent to the Biederharn polynomial[26] expansion employed by Herschbach and co-workers,[2] where the moments are related to the bipolar moments by a simple phase and scaling factor.

Shafer-Ray *et al.*[21] employ an alternative expansion to describe the CM correlated angular distribution (in the same coordinate system as that used here),

$$P(\omega_t,\omega_r)=\sum_{kq}\frac{[k]}{4\pi}\,\frac{1}{\sigma}\frac{d\sigma_{kq}}{d\omega_t}\,C_{kq}(\theta_r,\phi_r)^* \tag{7}$$

with the polarization dependent differential cross-sections (PDDCS) defined by

$$\frac{1}{\sigma}\frac{d\sigma_{kq}}{d\omega_t}=\int C_{kq}(\theta_r,\phi_r)P(\omega_t,\omega_r)d\omega_r. \tag{8}$$

Taking the complex conjugate of Eq. (8), it is readily shown that PDDCS satisfy the relation

$$\frac{1}{\sigma}\frac{d\sigma^*_{kq}}{d\omega_t}=(-1)^q\,\frac{1}{\sigma}\,\frac{d\sigma_{k-q}}{d\omega_t}. \tag{9}$$

Substitution of Eq. (5) into Eqs. (8) yields a relation between the CM frame bipolar moments and the PDDCS

$$\begin{aligned}\frac{1}{\sigma}\frac{d\sigma_{kq}}{d\omega_t}&=\frac{1}{4\pi}\sum_{Kk_1}(-1)^K[k_1]\\&\quad\times[K]^{1/2}\begin{pmatrix}k_1 & K & k\\ q & 0 & -q\end{pmatrix}h_0^K(k_1,k)C_{k_1-q}(\theta_t,0)\\&=\frac{1}{4\pi}\sum_{k_1}[k_1]s^{k_1}_{kq}C_{k_1-q}(\theta_t,0)\end{aligned} \tag{10}$$

with

$$s^{k_1}_{kq}=\sum_K(-1)^K[K]^{1/2}\begin{pmatrix}k_1 & K & k\\ q & 0 & -q\end{pmatrix}h_0^K(k_1,k).$$

A. Reflection symmetry in the scattering plane

Because of the choice of axes, the distribution of product AB inter-nuclear axes should be invariant to reflection in the $\mathbf{k},\mathbf{k}'$ xz plane, provided that the photon initiated reaction process is achiral. Since $\hat{\mathbf{j}}'$ behaves as a pseudovector, the x and z components of $\hat{\mathbf{j}}'$ change sign under reflection of the nuclear coordinates in the xz plane,[27] but the y component is invariant to reflection. As a consequence, we may write

$$P(\omega_t,\omega_r)\equiv P(\theta_t,\theta_r,\phi_r)=P(\theta_t,\pi-\theta_r,\pi-\phi_r). \tag{11}$$

Combining Eqs. (6) and (11), it can be concluded that

$$\frac{1}{\sigma}\frac{d\sigma_{kq}}{d\omega_t}=(-1)^{k+q}\frac{1}{\sigma}\,\frac{d\sigma_{k-q}}{d\omega_t}=(-1)^k\frac{1}{\sigma}\frac{d\sigma^*_{kq}}{d\omega_t} \tag{12}$$

and, using Eq. (9), these expressions yield

$$\begin{aligned}\frac{1}{\sigma}\frac{d\sigma_{kq+}}{d\omega_t}&=\frac{1}{\sigma}\frac{d\omega_{kq}}{d\omega_t}+\frac{1}{\sigma}\frac{d\sigma_{k-q}}{d\omega_t}\\&=0\quad k\ \text{even},\ q\ \text{odd or}\ k\ \text{odd},\ q\ \text{even},\end{aligned} \tag{13}$$

$$\begin{aligned}\frac{1}{\sigma}\frac{d\sigma_{kq-}}{d\omega_t}&=\frac{1}{\sigma}\frac{d\sigma_{kq}}{d\omega_t}-\frac{1}{\sigma}\frac{d\sigma_{k-q}}{d\omega_t}\\&=0\quad k\ \text{even},\ q\ \text{even or}\ k\ \text{odd},\ q\ \text{odd},\end{aligned}$$

which ensures that $P(\omega_t,\omega_r)$ is real. Finally, combining the above definitions with Eq. (10), the PDDCS may be rewritten, for later reference, in the more compact form

$$\frac{1}{\sigma}\frac{d\sigma_{kq\pm}}{d\omega_t}=\sum_{k_1}\frac{[k_1]}{4\pi}\,s^{k_1}_{kq\pm}C_{k_1-q}(\theta_t,0)$$

with

$$\begin{aligned}s^{k_1}_{kq\pm}&=\sum_K(-1)^K[K]^{1/2}\\&\quad\times\begin{pmatrix}k_1 & K & k\\ q & 0 & -q\end{pmatrix}\frac{[1\pm(-1)^{K+k_1+k+q}]}{1+\delta_{q0}}\,h_0^K(k_1,k),\end{aligned}$$

which may be evaluated using the expectation value expression

$$s^{k_1}_{kq\pm}=\langle C_{k_1q}(\theta_t,0)C_{kq}(\theta_r,0)[(-1)^qe^{iq\phi_r}\pm e^{-iq\phi_r}]\rangle,$$

where the angular brackets represent an average over *all* angles. Note that we have defined the PDDCS such that $(1/\sigma)(d\sigma_{k0\pm}/d\omega_t)=(1/\sigma)(d\sigma_{k0}/d\omega_t)$, and that the above equation, in conjunction with the planar symmetry constraints given in Eq. (13), implies that k_1+K must be even.

B. The moments of the k–k′ distribution

Integration of Eq. (5) over the angular coordinates of $\mathbf{j}'$ yields the moments of the $\mathbf{k}$–$\mathbf{k}'$ distribution, which correspond to the $h_0^K(k_1,k_2)$ moments with $k_2=0$. Hence, the differential cross-section is given by

$$\frac{1}{\sigma}\frac{d\sigma_{00}}{d\omega_t}\equiv P(\omega_t)=\frac{1}{4\pi}\sum_{k_1}[k_1]h_0^{k_1}(k_1,0)P_{k_1}(\cos\,\theta_t). \tag{14}$$

Therefore, the bipolar moments $h_0^k(k,0)$ are the expectation values of the Legendre moments of the usual differential cross section,

$$s^k_{00}=h_0^k(k,0)=\langle P_k(\cos\,\theta_t)\rangle. \tag{15}$$

C. The moments of the k–j′ distribution

The joint probability density function of the angles that define the direction of $\mathbf{j}'$, θ_r and ϕ_r, can be obtained by integrating the full $\mathbf{k}$–$\mathbf{k}'$–$\mathbf{j}'$ distribution over $\mathbf{k}'$ angles

$$P(\theta_r,\phi_r)\left(\equiv\frac{1}{\sigma}\frac{d\sigma}{d\omega_r}\right)$$

$$=\int P(\omega_t,\omega_r)d\omega_t$$

$$=\frac{1}{2}\sum_{kq}[k]C_{kq}(\theta_r,\phi_r)^*\int_{-1}^{1}\frac{1}{\sigma}\frac{d\sigma_{kq}}{d\omega_t}d(\cos\theta_t), \quad (16)$$

where $(1/\sigma)(d\sigma/d\omega_r)$ is the rotational solid angle differential cross-section.

Shafer-Ray *et al.*[21] defined polarization parameters

$$a_q^k=2\pi\int_{-1}^{1}\frac{1}{\sigma}\frac{d\sigma_{kq}}{d\omega_t}d(\cos\theta_t) \quad (17)$$

and in terms of these, we can recast the *rotational* solid angle differential cross section as

$$\frac{1}{\sigma}\frac{d\sigma}{d\omega_r}=\frac{1}{4\pi}\sum_{kq}[k]a_q^kC_{kq}(\theta_r,\phi_r)^*$$

$$=\frac{1}{4\pi}\sum_{k}\sum_{q\geqslant 0}[k][a_{q\pm}^k\cos q\phi_r$$

$$-a_{q\mp}^k\, i\sin q\phi_r]C_{kq}(\theta_r,0), \quad (18)$$

where the upper sign in the second line of Eq. (18) is associated with even q and the lower sign with odd q. The polarization parameters have the same properties as the polarization dependent differential cross sections, namely,

$$a_{q+}^k=0 \quad k \text{ even, } q \text{ odd or } k \text{ odd, } q \text{ even,}$$

$$a_{q-}^k=0 \quad k \text{ even, } q \text{ even or } k \text{ odd, } q \text{ odd,} \quad (19)$$

$$a_0^k=0 \quad \text{for } k \text{ odd,}$$

where the $a_{q\pm}^k$ are defined analogously to the PDDCS, given in Eq. (13) and, as with the PDDCS, $a_{0\pm}^k\equiv a_0^k$. The relation between the $a_{q\pm}^k$ parameters and the CM frame bipolar moments is given by

$$a_{q\pm}^k=\sum_{k_1}\frac{[k_1]}{2}s_{kq\pm}^{k_1}\int_{-1}^{+1}C_{k_1-q}(\theta_t,0)d(\cos\theta_t) \quad (20)$$

$$=\langle C_{k_1|q|}(\theta_r,0)2\cos q\phi_r\rangle \quad k \text{ even}$$

$$=i\langle C_{k_1|q|}(\theta_r,0)2\sin q\phi_r\rangle \quad k \text{ odd}$$

which for $q=0$ reduces to

$$a_0^k=h_0^k(0,k).$$

The $\mathbf{k}-\mathbf{j}'$ correlation is obtained by integrating Eq. (16) over ϕ_r,

$$P(\theta_r)=\int_0^{2\pi}P(\theta_r,\phi_r)d\phi_r=\frac{1}{2}\sum_k[k]a_0^kP_k(\cos\theta_r). \quad (21)$$

The coefficients of this distribution are expectation values of the Legendre polynomial expansion in $\cos\theta_r$ (where $\cos\theta_r=\hat{\mathbf{k}}\cdot\hat{\mathbf{j}}'$)

$$a_0^k=h_0^k(0,k)=\langle P_k(\cos\theta_r)\rangle. \quad (22)$$

As a consequence of Eq. (19), only the terms with even k are non-zero and the distribution of θ_r is even.

The distribution of dihedral angles, on the other hand, is given by

$$P(\phi_r)=\frac{1}{4\pi}\sum_{kq}[k]a_q^k\int_{-1}^{1}C_{kq}(\theta_r,\phi_r)^*\,d(\cos\theta_r) \quad (23)$$

or, more explicitly, as

$$P(\phi_r)=\frac{1}{4\pi}\sum_k\sum_{q\geqslant 0}[k][a_{q\pm}^k\cos q\phi_r-a_{q\mp}^k i\sin q\phi_r]$$

$$\times\int_{-1}^{1}C_{kq}(\theta_r,0)d(\cos\theta_r)$$

$$=\frac{1}{2\pi}\left(1+\sum_{\text{even }n\geqslant 2}a_n\cos n\phi_r\right.$$

$$\left.+\sum_{\text{odd }n\geqslant 1}b_n\sin n\phi_r\right). \quad (24)$$

The integrals over the spherical harmonics in Eq. (24) are zero unless $k+q$ is even and, in addition, all integrals with $q=0$ are zero, except for $k=0$, $q=0$, which is 2. This, in conjunction with rules for the $a_{q\pm}^k$, has the following repercussions for the $P(\phi_r)$:

(i) Only a_{q+}^k terms are involved in the expansion. Those involving a_{q-}^k are zero.

(ii) $P(\phi_r)$ can be expressed as a Fourier series with *only odd* terms in sines and *only even* terms in cosines [see the second line of Eq. (24)].

(iii) The a_n and b_n coefficients are themselves sums over even $k\geqslant n$ and odd $k\geqslant n$ terms, respectively, with only $k,q+$ contributions.

D. The moments of the k′–j′ distribution

If we contract the tensorial product in Eqs. (3) and (5) when $K=0$, which implies that $k_1=k_2=k$, the resulting angular distribution may be written

$$P(\theta_{tr})=\frac{1}{2}\sum_k[k]^{3/2}h_0^0(k,k)\sum_q C_{kq}(\theta_t,0)C_{kq}(\theta_r,\phi_r)^*. \quad (25)$$

Application of the spherical harmonic addition theorem[24] yields directly the moments of the $\mathbf{k}'-\mathbf{j}'$ distribution. The angle between these vectors, sometimes referred to as the helicity angle, is

$$\hat{\mathbf{k}}'\cdot\hat{\mathbf{j}}'=\cos\theta_{tr}=\cos\theta_r\cos\theta_t+\cos\phi_r\sin\theta_r\sin\theta_t.$$

Thus Eq. (25) becomes

$$P(\theta_{tr})=\frac{1}{2}\sum_k[k]^{3/2}h_0^0(k,k)P_k(\cos\theta_{tr}). \quad (26)$$

Therefore, the $h_0^0(k,k)$ CM frame bipolar moments are proportional to the expectation values of the Legendre polynomials in cos θ_{tr},

$$h_0^0(k,k)=\frac{1}{[k]^{1/2}}\langle P_k(\cos\ \theta_{tr})\rangle. \tag{27}$$

For the achiral systems under consideration, the $h_0^0(k,k)$ are zero if k is odd and the distribution is thus even.

E. Other moments

Integration of Eq. (5) over ϕ_r, and over the scattering plane azimuthal angle, renders the joint θ_t,θ_r probability density function, which corresponds to the information that can be obtained if only the projections $\hat{\mathbf{k}}\cdot\hat{\mathbf{j}}'$ and $\hat{\mathbf{k}}\cdot\hat{\mathbf{k}}'$ are measured

$$P(\theta_r,\theta_r)=2\pi\int P(\omega_t,\omega_r)d\phi_r$$

$$=\frac{1}{4}\sum_K\sum_{k_1k_2}(-1)^K[K]^{1/2}[k_1][k_2]h_0^K(k_1,k_2)$$

$$\times\begin{pmatrix}k_1 & K & k_2\\ 0 & 0 & 0\end{pmatrix}P_{k_1}(\cos\ \theta_t)P_{k_2}(\cos\ \theta_r) \tag{28}$$

which can be recast

$$P(\theta_t,\theta_r)=\frac{1}{4}\sum_{k_1k_2}[k_1][k_2]s_{k_20}^{k_1}P_{k_1}(\cos\ \theta_t)P_{k_2}(\cos\ \theta_r)$$

$$=2\pi\sum_{k_2}\frac{[k_2]}{2}\frac{1}{\sigma}\frac{d\sigma_{k_20}}{d\omega_t}P_{k_2}(\cos\ \theta_r), \tag{29}$$

where the moments of the distribution are given by

$$s_{k_20}^{k_1}=\langle P_{k_1}(\cos\ \theta_t)\cdot P_{k_2}(\cos\ \theta_r)\rangle. \tag{30}$$

Comparison of Eqs. (10) and (30) provides a simple meaning for the $s_{k_20}^{k_1}$ coefficients as those of the expansion of the PDDCS with $q=0$,

$$\frac{1}{\sigma}\frac{d\sigma_{k0}}{d\omega_t}=\frac{1}{4\pi}\sum_{k_1}[k_1]s_{k0}^{k_1}P_{k_1}(\cos\ \theta_t). \tag{31}$$

Since, according to Eq. (13), the PDDCS with $q=0$ are null unless k is even, only $s_{k_20}^{k_1}$ coefficients with even k_2 are different from zero. In addition, they can also be expressed as

$$s_{k0}^{k_1}=2\pi\int_{-1}^{1}\frac{1}{\sigma}\frac{d\sigma_{k0}}{d\omega_t}P_{k_1}(\cos\ \theta_t)d(\cos\ \theta_t) \tag{32}$$

and

$$s_{k0}^0=a_0^k=2\pi\int_{-1}^{1}\frac{1}{\sigma}\frac{d\sigma_{k0}}{d\omega_t}d(\cos\ \theta_t)$$

$$=h_0^k(0,k)=\langle P_k(\cos\ \theta_r)\rangle, \tag{33}$$

where the a_0^k are CM rotational alignment parameters.

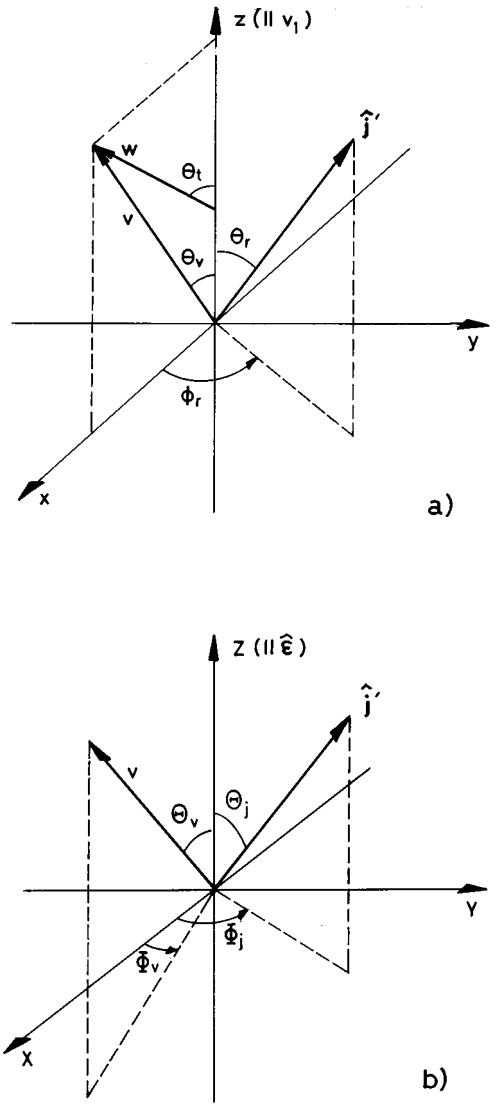

FIG. 2. (a) The v_1 frame coordinate system, as employed in the 1-D case described in Sec. III A. (b) The LAB frame coordinate system, which is the same for both the 1-D and 3-D transformation cases described in Secs. III A and III B.

III. THE LAB FRAME ANGULAR DISTRIBUTION

A. The 1-D case

As in the previous contribution,[19] to derive the product correlated LAB angular distribution we assume initially that the target molecule velocity, $\mathbf{v}_2$, is constrained to lie along $\mathbf{v}_1$, so that $\mathbf{k}\|\mathbf{v}_1$ and $k(\equiv v_r)=v_1\pm v_2$. This simple one dimensional approximation provides an excellent description of experiments which employ jet-cooled photolysis precursor and target molecule reagents and, as will be shown elsewhere,[23] is also a realistic approximation to the full three dimensional treatment, presented in the following section, required to describe many experiments conducted under thermal ''bulb'' conditions. The resulting expressions derived in this one dimensional treatment are also more readily compared with those obtained previously, most notably by

Shafer-Ray *et al.*,[21] which assume that photolysis precursor and target molecular motion may be neglected.

To transform from the CM to the LAB frame systems, it is convenient to define a v_1 *frame*, the z axis of which is defined along v_1 as illustrated in Fig. 2(a): note that in this ''1-D case,'' the coordinates of the product rotational angular momentum vector are unaffected by transformation of the translational coordinates from the CM to the v_1 frames. Provided that the products are probed at short (fixed) delays between the probe and photolysis lasers, the differential flux into product channel i in the v_1 frame will be proportional to the product AB_i number density, which may be written for a fixed v_1 and v_2 as[19]

$$\begin{aligned} I(\theta_v,\omega_r;v,v_1,v_2) &= R\sigma v_r P(\omega_t,\omega_r)\,\delta(w-w_i)\frac{\partial(w,\theta_t)}{\partial(v,\theta_v)} \\ &= R\sigma v_r P(\omega_t,\omega_r)\,\delta(w-w_i)\frac{v^2}{w_i^2} \\ &= R\sigma v_r P(\omega_t,\omega_r)\,\delta(\cos\theta_v-\cos\theta_v^i) \\ &\quad\times\frac{v}{w_i v_{cm}}, \end{aligned} \tag{34}$$

where R takes into account the number densities of the reagents and the reaction volume, and the angular coordinates of $\mathbf{v}$ in the v_1 frame are $\theta_v,\phi_v=\phi_t=0$.

On the other hand, the flux can be expressed in terms of v_1 *frame bipolar harmonics*, $B_0^K(k_1,k_2;\theta_v,\omega_r)$[28]

$$\begin{aligned} I(\theta_v,\omega_r;v,v_1,v_2) &= \frac{1}{8\pi}\sum_K\sum_{k_1}\sum_{k_2}[k_1] \\ &\quad\times[k_2]b_0^K(k_1,k_2;v) \\ &\quad\times B_0^K(k_1,k_2;\theta_v,\omega_r), \end{aligned} \tag{35}$$

where the new set of bipolar harmonics are given by

$$\begin{aligned} B_0^K(k_1,k_2;\theta_v,\omega_r) &= \sum_q(-1)^K[K]^{1/2}\begin{pmatrix} k_1 & K & k_2 \\ q & 0 & -q\end{pmatrix} \\ &\quad\times C_{k_1q}(\theta_v,0)C_{k_2-q}(\theta_r,\phi_r) \end{aligned} \tag{36}$$

and their corresponding bipolar moments by

$$\begin{aligned} b_0^K(k_1,k_2;v) &= \int B_0^K(k_1,k_2;\theta_v,\omega_r)^* \\ &\quad\times I(\theta_v,\omega_r;v,v_1,v_2)d(\cos\theta_v)d\omega_r \\ &= R\sigma v_r\sum_q(-1)^K[K]^{1/2}\begin{pmatrix} k_1 & K & k_2 \\ q & 0 & -q\end{pmatrix} \\ &\quad\times\frac{v}{w_i v_{cm}}\int d(\cos\theta_v)\,\delta(\cos\theta_v-\cos\theta_v^i) \\ &\quad\times C_{k_1q}(\theta_v,0)^*\int C_{k_2-q}(\theta_r,\phi_r)^* \\ &\quad\times P(\omega_t,\omega_r)d\omega_r, \end{aligned} \tag{37}$$

which reduces to

$$\begin{aligned} b_0^K(k_1,k;v) &= R\sigma v_r\sum_q(-1)^K[K]^{1/2}\begin{pmatrix} k_1 & K & k \\ q & 0 & -q\end{pmatrix} \\ &\quad\times\frac{v}{w_i v_{cm}}\,\frac{1}{\sigma}\frac{d\sigma_{kq}}{d\omega_t}C_{k_1-q}(\theta_v^i,0) \\ &= R\sigma v_r\sum_{q\geqslant 0}(-1)^K[K]^{1/2}\begin{pmatrix} k_1 & K & k \\ q & 0 & -q\end{pmatrix} \\ &\quad\times\frac{v}{w_i v_{cm}}\,\frac{1}{\sigma}\,\frac{d\sigma_{kq\pm}}{d\omega_t}C_{k_1-q}(\theta_v^i,0), \end{aligned} \tag{38}$$

where the plus sign goes with $K+k_1+k+q$ even and the minus sign with $K+k_1+k+q$ odd, and where $(1/\sigma)(d\sigma_{kq}/d\omega_t)$ is evaluated at the value of θ_t associated with θ_v^i and v. Because the v_1 frame probability distribution possesses a plane of symmetry, note that the sum of the indices, k_1+K, must be even, as was shown above to be the case for the CM frame bipolar moments.

The transformation of Eq. (35) from the v_1 frame to the LAB frame has been discussed previously[19] and is readily achieved by rotating the bipolar moments into the LAB frame, multiplying by the probability that the v_1 frame **z** axis ($\mathbf{v}_1$) has a specific orientation in the LAB frame (equivalent to the LAB frame velocity distribution of the atomic reagent) and integrating over all possible LAB orientations of the v_1 frame. For a fixed v_1 and v_2 the result is

$$\begin{aligned} &I(v,\Omega_v,\Omega_j;v_1,v_2) \\ &= \frac{1}{16\pi^2}\Bigg[\sum_k[k]^2 b_0^0(k,k;v)B_0^0(k,k;\Omega_v,\Omega_j) \\ &\quad+\frac{\beta}{5}\sum_{k_1,k_2}[k_1][k_2]b_0^2(k_1,k_2;v)B_0^2(k_1,k_2;\Omega_v,\Omega_j)\Bigg], \end{aligned} \tag{39}$$

where β is the CM translational anisotropy of the reagent atom, A, the bipolar moments are those of Eq. (38), and Ω_v and $\Omega_j\equiv(\theta_j,\phi_j)$ refer to the LAB angular coordinates of $\mathbf{v}$ and $\mathbf{j}'$, as defined in Fig. 2(b). The LAB frame distribution given by Eq. (39) is the appropriate one for jet cooled photon-initiated experiments conducted with a co-expanded beam of precursor and target reagent molecules. Note also that this equation is of the same form as that obtained for molecular photodissociation, the only differences being the definition of the v_1 frame bipolar moments and the presence of $\beta/2$ premultiplying the second term in Eq. (39), which ensures that the moments are referenced to $\mathbf{v}_1$ rather than μ (the electronic transition moment).

At this point it is possible to make a comparison with the previous work of Shafer-Ray *et al.*[21] They write the LAB angular distribution in terms of an expansion in LAB frame polarization parameters, $f_{kq}^{\epsilon}(\mathbf{v})$ (analogous to the LAB alignment parameters, $A_q^{(k)}$, employed in molecular photodissociation)[20,29]:

$$I(v,\Omega_v,\Omega_j,v_1,v_2)=\frac{1}{4\pi}\sum_{kq}[k]f_{kq}^{\epsilon}(\mathbf{v})C_{kq}(\Theta_j,\Phi_j)^*. \tag{40}$$

Comparison of Eqs. (39) and (40), using the definition of the v_1 frame bipolar moments given in Eq. (38), yields the following expression for the LAB frame polarization parameters:

$$\begin{aligned}f_{kq}^{\epsilon}(\mathbf{v})&=\int I(v,\Omega_v,\Omega_j;v_1,v_2)(-1)^q C_{k-q}(\Theta_j,\Phi_j)^*\,d\Omega_j\\&=\frac{1}{4\pi}\Bigg[[k]\begin{pmatrix}k&0&k\\q&0&-q\end{pmatrix}b_0^0(k,k;v)C_{k-q}(\Theta_v,\Phi_v)\\&\quad+\frac{\beta}{5^{1/2}}\sum_{k_1}[k_1]\begin{pmatrix}k_1&2&k\\q&0&-q\end{pmatrix}\\&\quad\times b_0^2(k_1,k;v)C_{k_1-q}(\Theta_v,\Phi_v)\Bigg].\end{aligned}$$

Substitution of expression (38) for the bipolar harmonics yields

$$\begin{aligned}f_{kq}^{\epsilon}(\mathbf{v})&=\frac{R\sigma v_r v}{4\pi w_i v_{cm}}\Bigg[C_{kq}(\Theta_v,\Phi_v)\sum_{q'}C_{kq'}(\theta_v^i,0)\frac{1}{\sigma}\frac{d\sigma_{kq'}}{d\omega_t}\\&\quad+\beta\sum_{k_1}\begin{pmatrix}k_1&2&k\\q&0&-q\end{pmatrix}(-1)^q C_{k_1 q}(\Theta_v,\Phi_v)\\&\quad\times\sum_{q'}\begin{pmatrix}k_1&2&k\\q'&0&-q'\end{pmatrix}C_{k_1-q'}(\theta_v^i,0)\frac{1}{\sigma}\frac{d\sigma_{kq'}}{d\omega_t}\Bigg].\end{aligned} \tag{41}$$

Although not given explicitly in the work of Shafer-Ray *et al.*,[21] it can be shown that the above expression is equivalent, apart from normalization, to that given by Eq. (59) of Ref. 21, provided that the Euler angles appearing in that equation are replaced by $\phi_R=0$, $\theta_R=\theta_{AB}^{\epsilon}$, and $\chi_R=\pi-\phi_{AB}^{\epsilon}$ (where the notation used is that of Ref. 21).

The integration over all possible magnitudes of v_1 and v_2 renders the final expressions for the LAB frame distribution

$$\begin{aligned}I(v,\Omega_v,\Omega_j)&=\frac{1}{16\pi^2}\Bigg[\sum_k[k]^2\overline{b_0^0(k,k;v)}B_0^0(k,k;\Omega_v,\Omega_j)\\&\quad+\frac{\beta}{5}\sum_{k_1,k_2}[k_1][k_2]\overline{b_0^2(k_1,k_2;v)}\\&\quad\times B_0^2(k_1,k_2;\Omega_v,\Omega_j)\Bigg],\end{aligned} \tag{42}$$

where the LAB speed-dependent averaged moments are given by[19]

$$\overline{b_0^K(k_1,k_2;v)}=\int\int f_K(v_1)g(v_2)b_0^K(k_1,k_2;v)v_1^2\,dv_1\,dv_2 \tag{43}$$

and the LAB speed distributions of v_1, $f_K(v_1)$, and v_2, $g(v_2)$, have been given explicitly in a previous contribution.[9] For the case of photon-initiated bimolecular reaction studies under room temperature conditions $g(v_2)$ is simply a 1-D Maxwell–Boltzmann distribution and $f_K(v_1)$ takes explicit account of the thermal motion of the precursor molecule and the possible spread in recoil velocities associated with the photodissociation of a polyatomic molecule. We note that the LAB speed distribution of the product molecules, $W(v)v^2$, introduced in the previous publication,[19] and defined as

$$\begin{aligned}\overline{b_0^0(0,0;v)}&=\int\int f_0(v_1)g(v_2)b_0^0(0,0;v)v_1^2\,dv_1\,dv_2\\&=W(v)v^2\end{aligned} \tag{44}$$

was factored out of Eq. (42) and $\overline{b_0^0(0,0;v)}$ was redefined as unity. Here, as previously, the LAB speed distribution is normalized to the total reactive flux, $\langle v_r\sigma\rangle$.

In principle, the sums over the indices k, k_1, and k_2 are infinite, subject only to triangle conditions of the 3-J symbol defined in the bipolar harmonics. However, if the photoinitiated reaction process is non-chiral and the reaction products are probed using linearly polarized light via 1+1 laser induced fluorescence (LIF) in the commonly employed geometries,[20,29] the k indices are restricted to even values only and the expansion is limited to the first ten even bipolar moments, $\overline{b_0^K(k_1,k_2;v)}$. Table I provides the coefficients [as given by Eq. (38)] of the polarization dependent differential cross-sections appearing in the integrands of the six most important of these bipolar moments. Table I also includes, for later reference, the simple renormalization factors used to relate the $\overline{b_0^K(k_1,k_2;v)}$ moments to the more commonly employed $\overline{\beta_0^K(k_1,k_2;v)}$ moments.

B. The 3-D case

To obtain the LAB distribution in the more general case, when $\mathbf{v}_1$ and $\mathbf{v}_2$ are not constrained to lie parallel to one another, we define a modified v_1 reference frame with its Z axis in the direction of $\mathbf{v}_1$ and its X axis constrained in the v_1-v_2 plane (i.e., $\mathbf{k}$ lines in this plane), as shown in Fig. 3. In this frame, $\mathbf{k}$ makes an angle θ_k with the z-axis, and the xz CM scattering plane makes an angle ϕ_t with the XZ v_1 plane (see Fig. 3—note that for the present purposes this angle is defined such that $\phi_t\rightarrow\phi_v$ when $\theta_k\rightarrow 0$).

The product differential flux for a fixed Newton triangle and a single velocity $\mathbf{v}$ of the products (again proportional to number density at short, fixed delay times) in the v_1 frame may now be written as (see the Appendix and Ref. 30)

TABLE I. The relationship between commonly determined 1-D ''moving'' frame bipolar moments, and the polarization dependent differential cross-sections. To obtain normalization, each of the latter should be multiplied by the common factor of $R\sigma v v_r / w_i v_{cm}$.

	Coefficients			
Bipolar moment	$\frac{1}{\sigma}\frac{d\sigma_{00}}{d\omega_t}$	$\frac{1}{\sigma}\frac{d\sigma_{20}}{d\omega_t}$	$\frac{1}{\sigma}\frac{d\sigma_{21-}}{d\omega_t}$	$\frac{1}{\sigma}\frac{d\sigma_{22+}}{d\omega_t}$
$\beta_0^0(0,0)$ $[\equiv b_0^0(0,0)]$	1	0	0	0
$\beta_0^2(2,0)$ $[\equiv b_0^2(2,0)]$	$C_{20}(\theta_v^i,0)$	0	0	0
$\beta_0^2(0,2)$ $[\equiv b_0^2(0,2)]$	0	1	0	0
$\beta_0^0(2,2)[\equiv\sqrt{5}b_0^0(2,2)]$	0	$C_{20}(\theta_v^i,0)$	$C_{21}(\theta_v^i,0)$	$C_{22}(\theta_v^i,0)$
$\beta_0^2(2,2)\left[\equiv\sqrt{\frac{7}{2}}b_0^2(2,2)\right]$	0	$-C_{20}(\theta_v^i,0)$	$-\frac{1}{2}C_{21}(\theta_v^i,0)$	$C_{22}(\theta_v^i,0)$
$\beta_0^2(4,2)\left[\equiv\sqrt{\frac{7}{2}}b_0^2(4,2)\right]$	0	$C_{40}(\theta_v^i,0)$	$\sqrt{\frac{5}{6}}C_{41}(\theta_v^i,0)$	$\sqrt{\frac{5}{12}}C_{42}(\theta_v^i,0)$

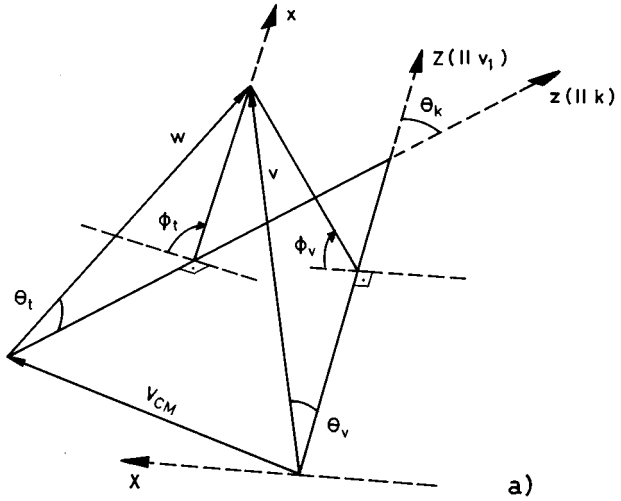

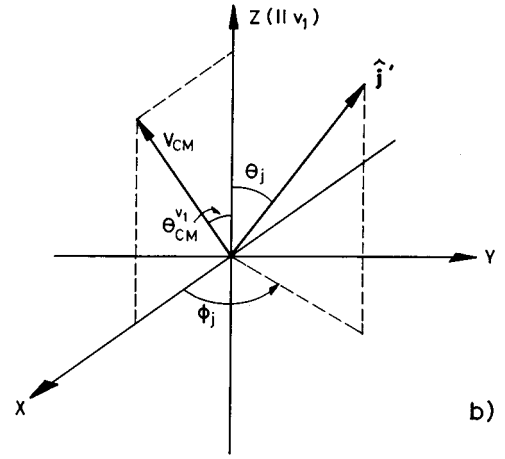

FIG. 3. (a) The coordinates and Euler angles describing the transformation from the CM to the v_1 frames in the 3-D case of Section III B. (b) The v_1 frame coordinates employed in the 3-D integration case of Section III B.

$$I(\omega_v,\omega_j;v,\mathbf{v}_1,\mathbf{v}_2)=R\sigma v_r\sum_{kq}\frac{[k]}{4\pi}\sum_{q'}D^k_{q'q}(-\phi_t,\theta_k,0)\times\frac{1}{\sigma}\frac{d\sigma_{kq'}}{d\omega_t}C_{kq}(\theta_j,\phi_j)^*\times\delta(\cos\theta_v-\cos\theta_v^i)\left|\frac{d\cos\theta_v}{dw_i}\right|\frac{v^2}{w_i^2},\tag{45}$$

where ω_v,ω_j describe the angular coordinates of $\mathbf{v}$ and $\mathbf{j}'$ in the v_1 frame and the Jacobian employed is defined

$$\left|\frac{d\cos\theta_v}{dw_i}\right|^{-1}=\left|\frac{v_{cm}v}{w_i}\left(\frac{\cos\theta_v}{\sin\theta_v}\cos\phi_v\sin\theta_{cm}^{v_1}-\cos\theta_{cm}^{v_1}\right)\right|,\tag{46}$$

where $\theta_{cm}^{v_1}$ is the angle between the CM velocity vector, $\mathbf{v}_{cm}$, and $\mathbf{v}_1$. [We note that in the previous work[19] the Jacobian erroneously included an extra factor of 2 in front of the first term in Eq. (46).]

As in the 1-D case, the flux can be expressed as a series expansion of v_1 *frame bipolar harmonics*, $B_Q^K(k_1,k_2;\omega_v,\omega_j)$[31]

$$I(\omega_v,\omega_j;v,\mathbf{v}_1,\mathbf{v}_2)=\frac{1}{16\pi^2}\sum_{KQ}\sum_{k_1k_2}[k_1]\times[k_2]b_Q^K(k_1,k_2;v)\times B_Q^K(k_1,k_2;\omega_v,\omega_j)\tag{47}$$

which are given by

$$B_Q^K(k_1,k_2;\omega_v,\omega_j)=\sum_{q_1}(-1)^{K-Q}[K]^{1/2}\times\begin{pmatrix}k_1 & K & k_2\\ q_1 & -Q & q_2\end{pmatrix}C_{k_1q_1}(\theta_v,\phi_v)\times C_{k_2q_2}(\theta_j,\phi_j), \tag{48}$$

and the moments associated with them by

$$b_Q^K(k_1,k_2;v)=\int\int B_Q^K(k_1,k_2;\omega_v,\omega_j)^*\times I(\omega_v,\omega_j;v,\mathbf{v}_1,\mathbf{v}_2)d\omega_v\,d\omega_j. \tag{49}$$

Substitution of Eq. (46) into Eq. (49) yields

$$b_Q^K(k_1,k_2;v)=R\sigma v_r\int\int\sum_{q_1}(-1)^{K-Q}[K]^{1/2}\begin{pmatrix}k_1 & K & k_2\\ q_1 & -Q & q_2\end{pmatrix}C_{k_1q_1}(\theta_v,\phi_v)^*(-1)^{q_2}C_{k_2-q_2}(\theta_j,\phi_j)\times\sum_{kq}\frac{[k]}{4\pi}\sum_{q'}D^k_{q'q}(-\phi_t,\theta_k,0)\frac{1}{\sigma}\frac{d\sigma_{kq'}}{d\omega_t}C_{kq}(\theta_j,\phi_j)^*\,\delta(\cos\theta_v-\cos\theta_v^i)\left|\frac{d\cos\theta_v}{dw_i}\right|\frac{v^2}{w_i^2}\,d\omega_v\,d\omega_j.$$

Integration over ω_j and θ_v renders

$$b_Q^K(k_1,k;v)=R\sigma v_r\int\sum_{q_1}(-1)^K[K]^{1/2}\begin{pmatrix}k_1 & K & k\\ q_1 & -Q & -q\end{pmatrix}C_{k_1-q_1}(\theta_v^i,0)\times\sum_{q'}d^k_{q'q}(\theta_k)e^{-iq_1\phi_v}e^{iq'\phi_t}\frac{1}{\sigma}\frac{d\sigma_{kq'}}{d\omega_t}\left|\frac{d\cos\theta_v^i}{dw_i}\right|\frac{v^2}{w_i^2}\,d\phi_v. \tag{50}$$

As in the 1-D case, the v_1 frame distribution possesses a plane of symmetry, and therefore the sum of the indices, k_1+K, must be even. Specializing Eq. (50) for $Q=0$, yields

$$b_0^K(k_1,k;v)=R\sigma v_r\int\sum_{q}(-1)^K[K]^{1/2}\begin{pmatrix}k_1 & K & k\\ q & 0 & -q\end{pmatrix}C_{k_1-q}(\theta_v^i,0)\times\sum_{q'}d^k_{q'q}(\theta_k)e^{-iq\phi_v}e^{iq'\phi_t}\frac{1}{\sigma}\frac{d\sigma_{kq'}}{d\omega_t}\left|\frac{d\cos\theta_v^i}{dw_i}\right|\frac{v^2}{w_i^2}\,d\phi_v. \tag{51}$$

For the bipolar moments with *even* indices, this expression can be expressed more explicitly as

$$b_0^K(k_1,k;v)=R\sigma v_r\int\sum_{q\geqslant 0}(-1)^K[K]^{1/2}\begin{pmatrix}k_1 & K & k\\ q & 0 & -q\end{pmatrix}C_{k_1-q}(\theta_v^i,0)\times\sum_{q'\geqslant 0}\frac{[d^k_{q'q}(\theta_k)\cos(q'\phi_t-q\phi_v)+(-1)^{q'}d^k_{-q'q}(\theta_k)\cos(q'\phi_t+q\phi_v)]}{(1+\delta_{q0})}\frac{1}{\sigma}\frac{d\sigma_{kq'\pm}}{d\omega_t}\left|\frac{d\cos\theta_v^i}{dw_i}\right|\frac{v^2}{w_i^2}\,d\phi_v, \tag{52}$$

where the plus sign in $(1/\sigma)(d\sigma_{kq'\pm}/d\omega_t)$ is associated with q' even, the minus sign with q' odd and, as previously,

$$\frac{1}{\sigma}\frac{d\sigma_{k0\pm}}{d\omega_t}=\frac{1}{\sigma}\frac{d\sigma_{k0}}{d\omega_t}. \tag{53}$$

Notice that Eqs. (47), (51), and (52) reduce in the 1-D limit, where $\theta_k\to 0$ and $\phi_t\to\phi_v$, to Eqs. (35) and (38). It is stressed at this point that Eq. (47) (suitably averaged over reagent velocity distributions), together with the definitions of the bipolar moments, is quite general and would be suitable for the analysis of data obtained from crossed-molecular beam experiments, for example.

As in the 1-D case, to obtain the LAB flux, we integrate Eq. (47) over the LAB distribution of $\mathbf{v}_1$ and $\mathbf{v}_2$. The integration over the angular coordinates of v_1 may be performed analytically, as in the 1-D case, yielding the final expression for the angular distribution

TABLE II. The relationship between commonly determined 3-D v_1 frame bipolar moments, and the polarization dependent differential cross-sections. To obtain normalization, each of the latter should be multiplied by the $R\sigma v_r v^2/w_i^2 \left| d\ \cos\ \theta_v/dw_i \right|$.

	Coefficients			
Bipolar Moments	$\frac{1}{\sigma}\frac{d\sigma_{00}}{d\omega_t}$	$\frac{1}{\sigma}\frac{d\sigma_{20}}{d\omega_t}$	$\frac{1}{\sigma}\frac{d\sigma_{21-}}{d\omega_t}$	$\frac{1}{\sigma}\frac{d\sigma_{22+}}{d\omega_t}$
$\beta_0^0(0,0)$	1	0	0	0
$\beta_0^2(2,0)$	$C_{20}(\theta_v^i,0)$	0	0	0
$\beta_0^2(0,2)$	0	$d_{00}^2(\theta_k)$	$\cos\ \phi_t d_{10}^2(\theta_k)$	$\cos 2\phi_t d_{20}^2(\theta_k)$
$\beta_0^0(2,2)$	0	$\Sigma_{q\geqslant 0} C_{2q}(\theta_v^i,0)\cos q\phi_v \times \frac{2d_{0q}^2(\theta_k)}{1+\delta_{q0}}$	$\Sigma_{q\geqslant 0} C_{2q}(\theta_v^i,0) \times \frac{d_{1q}^2(\theta_k)\cos(\phi_t-q\phi_v)-d_{-1q}^2(\theta_k)\cos(\phi_t+q\phi_v)}{1+\delta_{q0}}$	$\Sigma_{q\geqslant 0} C_{2q}(\theta_v^i,0) \times \frac{d_{2q}^2(\theta_k)\cos(2\phi_t-q\phi_v)+d_{-2q}^2(\theta_k)\cos(2\phi_t+q\phi_v)}{1+\delta_{q0}}$
$\beta_0^2(2,2)$	0	$\Sigma_{q\geqslant 0}\left(\frac{q^2-2}{2}\right) C_{2q}(\theta_v^i,0) \times\cos(q\phi_v)\frac{2d_{0q}^2(\theta_k)}{1+\delta_{q0}}$	$\Sigma_{q\geqslant 0}\left(\frac{q^2-2}{2}\right) C_{2q}(\theta_v^i,0) \times \frac{d_{1q}^2(\theta_k)\cos(\phi_t-q\phi_v)-d_{-1q}^2(\theta_k)\cos(\phi_t+q\phi_v)}{1+\delta_{q0}}$	$\Sigma_{q\geqslant 0}\left(\frac{q^2-2}{2}\right) C_{2q}(\theta_v^i,0) \times \frac{d_{2q}^2(\theta_k)\cos(2\phi_t-q\phi_v)+d_{-2q}^2(\theta_k)\cos(2\phi_t+q\phi_v)}{1+\delta_{q0}}$
$\beta_0^2(4,2)$	0	$\Sigma_{q\geqslant 0}\frac{1}{12}[(16-q^2)(9-q^2)]^{1/2} C_{4q}(\theta_v^i,0) \times\cos(q\phi_v)\frac{2d_0^2(\theta_k)}{1+\delta_{q0}}$	$\Sigma_{q\geqslant 0}\ \frac{1}{12}[(16-q^2)(9-q^2)]^{1/2} C_{4q}(\theta_v^i,0) \times \frac{d_{1q}^2(\theta_k)\cos(\phi_t-q\phi_v)-d_{-1q}^2(\theta_k)\cos(\phi_t+q\phi_v)}{1+\delta_{q0}}$	$\Sigma_{q\geqslant 0}\ \frac{1}{12}[(16-q^2)(9-q^2)]^{1/2} C_{4q}(\theta_v^i,0) \times \frac{d_{2q}^2(\theta_k)\cos(2\phi_t-q\phi_v)+d_{-2q}^2(\theta_k)\cos(2\phi_t+q\phi_v)}{1+\delta_{q0}}$

$$I(v,\Omega_v,\Omega_j) = \frac{1}{16\pi^2}\left[\sum_k [k]^2 \overline{b_0^0(k,k;v)} B_0^0(k,k;\Omega_v,\Omega_j) + \frac{\beta}{5}\sum_{k_1,k_2}[k_1][k_2]\overline{b_0^2(k_1,k_2;v)} B_0^2(k_1,k_2;\Omega_v,\Omega_j)\right], \tag{54}$$

where the LAB speed-dependent averaged moments are now given by

$$\overline{b_0^K(k_1,k_2;v)} = \int\int\int\int f_k(v_1) g(v_2) \times b_0^K(k_1,k_2;v) v_1^2 v_2^2\ dv_1\ dv_2\ d\Omega_{v_2}. \tag{55}$$

As in the 1-D case, the integrands of the LAB moments most commonly encountered in 1+1 LIF studies,[19,21] specifically the coefficients of the polarization dependent differential cross-sections appearing in the v_1-frame moments of Eq. (52) are presented in Table II.

IV. SIMULATIONS

A. Polarization dependent differential cross-sections

To help provide a more physical interpretation of the PDDCS, we provide below some limiting values of four of the most commonly encountered moments under extreme polarization conditions. Second, for the first time we present, mainly for illustrative purposes, quasi-classical trajectory (QCT) calculated PDDCS for the reaction $O(^1D)+HD$. Further details of the latter calculations can be found in Refs. 32 and 33: The latter paper will also discuss in more detail the relationship between the PDDCS and the $O(^1D)+HD$ reaction mechanism.

1. Limiting values of the PDDCS

The PDDCS are normalized such that integration over scattering angles, $\cos\theta_t$, renders the alignment parameters, $a_{q\pm}^k$, via Eqs. (17) and (20). As shown in Sec. II, the polarization parameters describe the anisotropy of angular momentum distribution and are simply expectation values of the appropriate modified spherical harmonic

$$a_{q\pm}^k = \langle C_{kq}(\theta_r,0)[e^{iq\phi_r} \pm (-1)^q e^{-iq\phi_r}]\rangle. \tag{56}$$

Likewise, it can be shown that the renormalized PDDCS, the quotient of the PDDCS and the differential cross-section, may be expressed as *conditional* expectation values for a given CM scattering angle, $\cos\theta_t$

$$\frac{\frac{1}{\sigma}\frac{d\sigma_{kq\pm}}{d\omega_t}}{\frac{1}{\sigma}\frac{d\sigma_{00}}{d\omega_t}} = \langle C_{kq}(\theta_r,0)[e^{iq\phi_r} \pm (-1)^q e^{-iq\phi_r}] | \cos\ \theta_t\rangle. \tag{57}$$

Arguments and some limiting values of the four moments most commonly encountered are given in Table III: Note that even the limited number of polarization parameters presented in this table provide rich dynamical information about the rotational polarization of the reaction product, and its CM scattering angle dependence.

TABLE III. Arguments and limiting values of some of the alignment parameters and renormalized PDDCS (see the text). The left hand column gives the k,q index of the moment of interest and the limiting values are listed for the given (θ_r,ϕ_r) angles, expressed in degrees.

		Limiting values (θ_r,ϕ_r)						
$kq\pm$	Argument	0,0	0,90	45,0	45,90	45,180	90,0	90,90
0 0	1	1	1	1	1	1	1	1
2 0	$P_2(\cos\theta_r)$	1	1	$\frac{1}{4}$	$\frac{1}{4}$	$\frac{1}{4}$	$-\frac{1}{2}$	$-\frac{1}{2}$
2 1−	$2\,C_{21}(\theta_r,0)\cos\phi_r$	0	0	$-\sqrt{\frac{3}{2}}$	0	$+\sqrt{\frac{3}{2}}$	0	0
2 2+	$2\,C_{22}(\theta_r,0)\cos 2\phi_r$	0	0	$+\sqrt{\frac{3}{8}}$	$-\sqrt{\frac{3}{8}}$	$+\sqrt{\frac{3}{8}}$	$+\sqrt{\frac{3}{2}}$	$-\sqrt{\frac{3}{2}}$

2. QCT calculated PDDCS for the reaction $O(^1D)+HD$

As an illustrative example, QCT calculated PDDCS for the reaction $O(^1D)+HD\rightarrow OH(v'=0)+D$ are presented in Figs. 4–6. The calculations have been performed using the Schinke–Lester surface,[35] and each alignment and/or PDDCS parameter has been evaluated by weighting the trajectories in accord with the expectation value equations (56) and (57): The general procedure employed is an extension of that presented previously in Ref. 36, a full account of which will be given elsewhere.[33] PDDCS for the $q=0$ moments with $k\leqslant 4$ are shown in Fig. 4; that for $k=0$ is simply the $(\mathbf{k},\mathbf{k}')$ differential cross-section, which is broad and appears to display forward-backward symmetry (see, however, Ref. 32 for a more detailed discussion of this behavior). More readily interpretable are the renormalized PDDCS shown in Fig. 5 since, as mentioned above, these represent conditional expectation values of the modified spherical harmonics at fixed CM scattering angle. The behavior of the $(k,q)=(2,0)$ moment, whose value is the expectation value of the second Legendre moment, is perhaps most readily interpreted: The values close to $-1/2$ at $\cos\theta_t=\pm 1.0$ suggest that $\mathbf{j}'$ is preferentially polarized perpendicular to the reagent relative velocity when the fragment (OH) is scattered forward or backwards parallel or antiparallel to $\mathbf{k}$. This interpretation is reinforced by the $(k,q)=(4,0)$ moment, which also tends to the limiting values for $\mathbf{k}\perp\mathbf{j}'$ at scattering angles close to $\theta_t=0$ and 180°. Away from these scattering angles, both the $(k,q)=(2,0)$ and (4,0) renormalized PDDCS become close to zero, suggesting that the rotational angular momentum distribution in $\cos\theta_r$ is more isotropic for sideways scattering.

The PDDCS for $k=2$, $q\neq 0$, together with their renormalized values, are shown in Fig. 6. It is clear that the expectation values of these moments are far from the limiting values given in Table III, perhaps not surprisingly for this insertion dominated reaction.[32,37] Note that at the extremes of forward and/or backward scattering, the $k,q=2,1-$ and

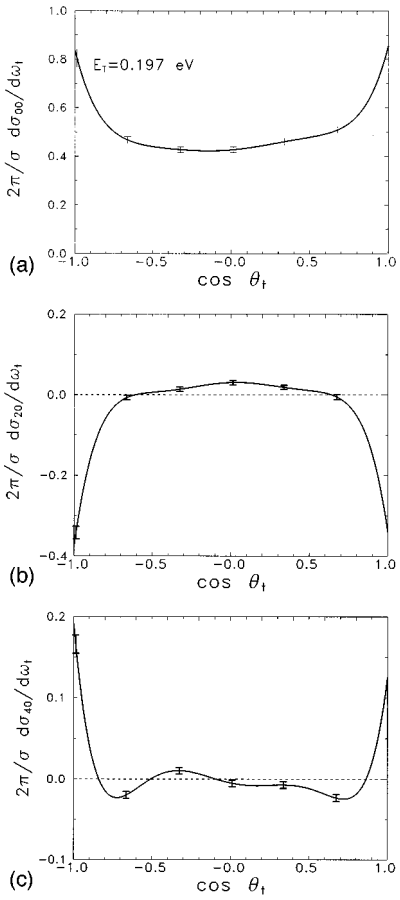

FIG. 4. PDDCS with $(k,q)=(0,0)$ (a), (2,0) (b) and (4,0) (c) for the $O(^1D)+HD\rightarrow OH(v'=0)+D$ reaction. That for $k=0$ is simply the $OH(v'=0)$ state-resolved differential $\mathbf{k},\mathbf{k}'$ cross-section (Ref. 32).

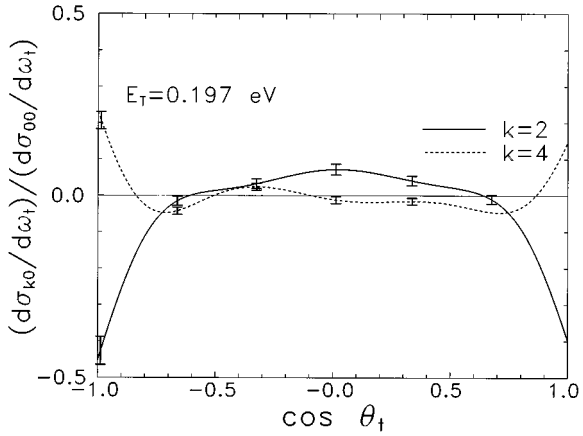

FIG. 5. Renormalized PDDCS, i.e., the PDDCS divided by the differential cross-section, with $(k,q)=(2,0)$ and (4,0) for the $O(^1D)+HD\rightarrow OH(v'=0)+D$ reaction.

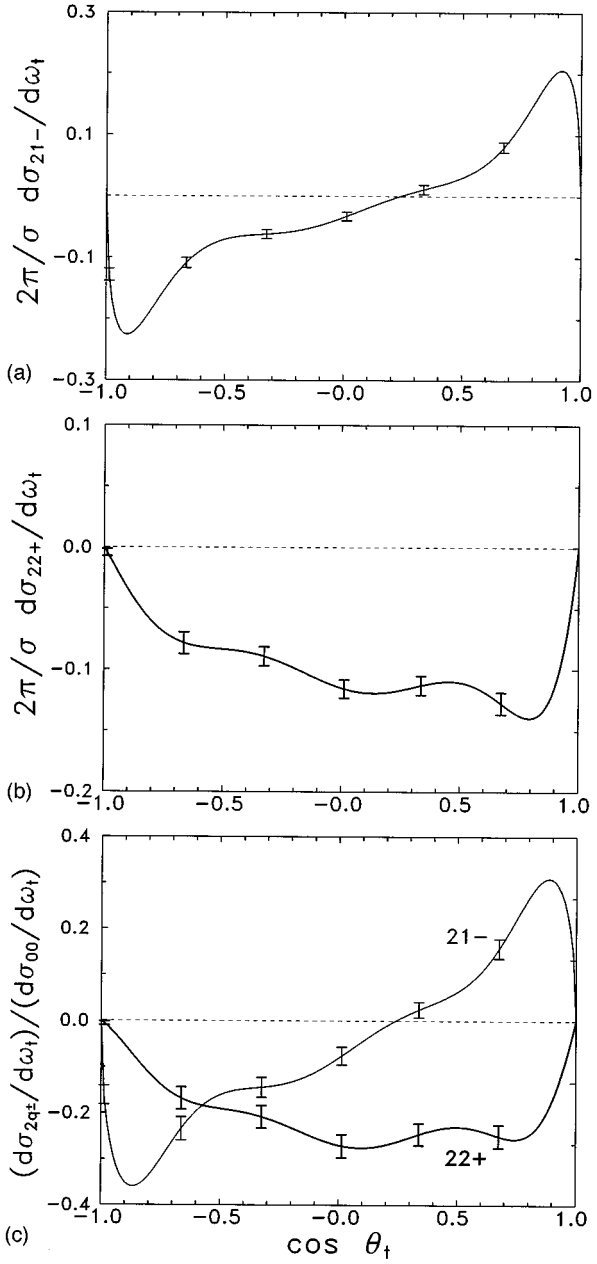

FIG. 6. PDDCS ((a) and (b)) and renormalized PDDCS (c) with $(k,q\pm)=2,1-)$ and $(2,2+)$ for the $O(^1D)+HD\rightarrow OH(v'=0)+D$ reaction.

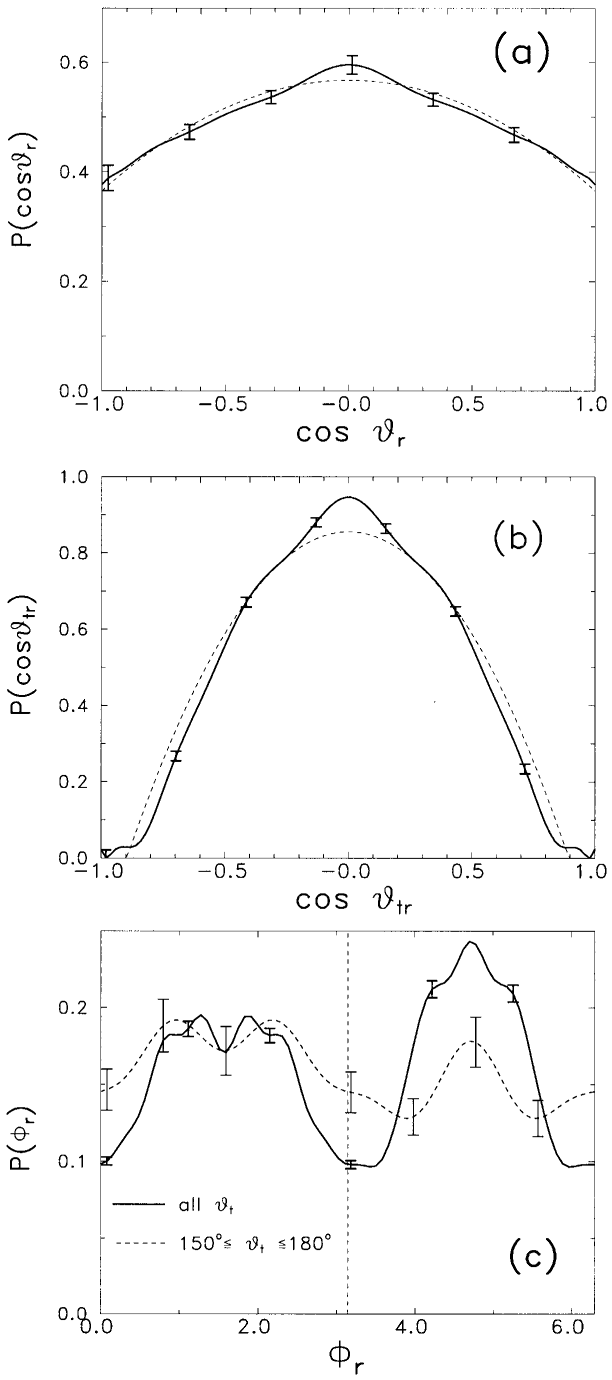

FIG. 7. (a) The $P(\cos\theta_r)$ $\mathbf{k},\mathbf{j}'$ distribution for the $O(^1D)+HD\rightarrow OH(v'=0)+D$ reaction, averaged over all scattering angles. The solid line is the distribution function obtained employing Legendre moments with k up to 14, which is sufficient for very good convergence, whilst the dashed line is that employing only the $k=0$ and 2 moments. (b) The $P(\cos\theta_{tr})$ $\mathbf{k}',\mathbf{j}'$ distribution, averaged over all scattering angles for the same reaction as in (a). The solid line is the distribution function obtained employing Legendre moments with k up to 16, which yields good convergence to the trajectory data, whilst the dashed line is that employing only the $k=0$ and 2 moments. (c) The $P(\phi_r)$ distribution. The solid line is the distribution function obtained averaging over all scattering angles, whilst the dashed line is the conditional distribution function obtained by averaging only over the angles $\theta_t=150°$ to 180°. The plots were obtained using the expansion given in Eq. (24) with k up to 7, which again was sufficient for good convergence.

2,2+ PDDCS are necessarily zero. At these limiting scattering angles, the $\mathbf{k},\mathbf{k}'$ scattering plane is not defined and all moments with $q\neq 0$ must be zero. More interesting is the behavior of the $q\neq 0$ moments at scattering angles away from the extreme forward and backward directions, since these provide information on the ϕ_r dihedral angle distribution. Unlike the $q=0$ PDDCS, those with $q\neq 0$ are non-zero at scattering angles away from $\theta_t=0$ and 180°, clearly indicating that, although not strongly polarized, the $P(\theta_r,\phi_r)$ distribution is not isotropic for sideways scattered products. The variations in the $k=2$ renormalized PDDCS with scattering angle reflect changes in the rotational polarization with scattering angle, as will be further illustrated below, and

suggests that the PDDCS for the $O(^1D)+HD$ reaction contain important dynamical information.

A more graphic representation of the angular momentum polarization is obtained by plotting angular distributions over $\cos\theta_r$, $\cos\theta_{tr}$ or ϕ_r angles. The first two distributions, once averaged over all scattering angle, represent the $\mathbf{k},\mathbf{j}'$ and $\mathbf{k}',\mathbf{j}'$ correlations, respectively, and are shown in Figs. 7(a) and 7(b). The trajectory calculations employ Legendre moment expansions up to $k=14$ and 16, respectively, but as shown in the two figures, the main features of both distributions are reasonably well captured with just the first two ($k=0$ and 2) even Legendre moments. Both distributions peak at θ_r or θ_{tr} angles close to 90° (remember that these distribution functions are even and thus must be symmetric with respect to 90°). Note, however, that $P(\cos\theta_{tr})$, which reflects motions in the exit channel, is both considerably more aligned and more confined to angles about 90° than $P(\cos\theta_r)$ (these differences in alignment are clearly reflected by the values of the second Legendre moments for the two distributions of -0.285 and -0.054, respectively).

As already stressed above, the PDDCS illustrated in Figs. 4 to 6 contain more information about the polarization of the products than that shown in Figs. 7(a) and 7(b), since they also reveal how this polarization varies with scattering angle. We illustrate one aspect of this scattering angle dependence in Fig. 7(c), in which is compared the distribution in ϕ_r (averaged overall scattering angles) with the *conditional* probability distribution, $P(\phi_r|-1.0\leqslant\cos\theta_t\leqslant-\sqrt{3}/2)$. Unlike the distributions $P(\cos\theta_r)$ and $P(\cos\theta_{tr})$, the dihedral angle distribution functions contain *odd k* moments: the data shown in Fig. 7(c) demonstrates that these moments are nonzero for the $O(^1D)+HD$ reaction. This bias in the dihedral angular distribution, and its dynamical implications, will be explored in more detail elsewhere.[33] We note in passing, however, that the importance of determining the dihedral angle distribution has been emphasized previously by Herschbach and co-workers,[38] although primarily in the context of reactions which proceed via statistical long-lived complexes, for which the dihedral angle distribution is symmetric about $\phi_r=\pi$.

Finally, and perhaps most revealing of all, we present the angular distribution of the rotational vectors in the form of polar plots in θ_r and ϕ_r, either averaged over all scattering angles [Fig. 8(a)] or averaged over a restricted range of scattering angles, corresponding to $-1.0\leqslant\cos\theta_t\leqslant-\sqrt{3}/2$ [Fig. 8(b)]. The calculations employ expansions in all (k,q) moments up to $k=7$, but once again, many of the important features are captured if only moments up to $k=2$ are included. This fact is illustrated in Fig. 9, which shows fits to the same trajectory data as in Fig. 8, but employing expansions including only the first four *even k* polarization parameters most amenable to experimental determination (i.e., those identified in Tables I to III). Both sets of plots suggest that, on average, the $OH(v'=0)$ fragments are preferentially polarized *perpendicular* to the $\mathbf{k},\mathbf{k}'$ plane, although for backward scattered products $P(\theta_r,\phi_r)$ shows considerable probability for rotational polarization *in* the $\mathbf{k},\mathbf{k}'$plane. Note that, as with the $P(\phi_r)$ distribution, those shown in Figs. 8 are not symmetric about $\phi_r=\pi$, reflecting the nonzero values of the PDDCS and $a^k_{q\pm}$ moments with odd k.

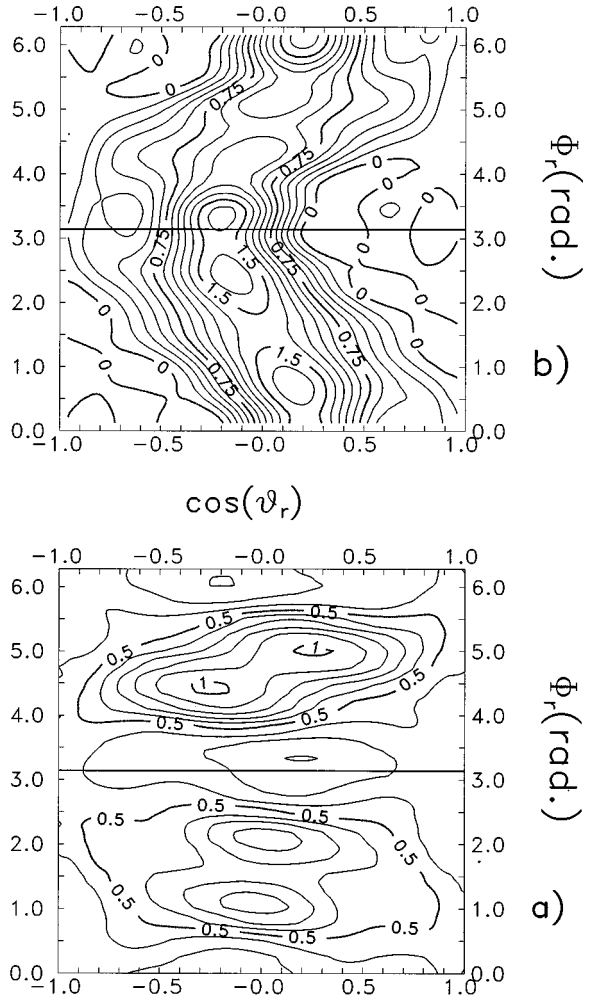

FIG. 8. Polar plots of the $P(\theta_r,\phi_r)$ distribution obtained using all moments up to $k=7$, and averaged either over all scattering angles (a), or just over the backward scattering angles $\theta_t=150°$ to 180° (b).

B. LAB frame bipolar moments

The QCT calculated PDDCS shown in the preceeding section may be employed in simulations of LAB frame bipolar moments using either the 1-D approximation or the full 3-D integration over reagent velocities. The present focus is to illustrate how the PDDCS presented above would manifest themselves in LAB frame bipolar moment measurements using, for example, 1+1 LIF Doppler-resolved spectroscopy. The sensitivity of the LAB frame measurements to CM polarization will be dependent on experimental details as well as on the kinematics and energetics of the reaction under study, and a more detailed discussion of this topic is deferred to a forthcoming paper.[23] Here we present simulated ''composite'' Doppler broadened profiles[19,34] that would be obtained via 1+1 LIF or REMPI probing of the reaction products under room temperature conditions, although we stress that the equations developed in the preceeding sections can

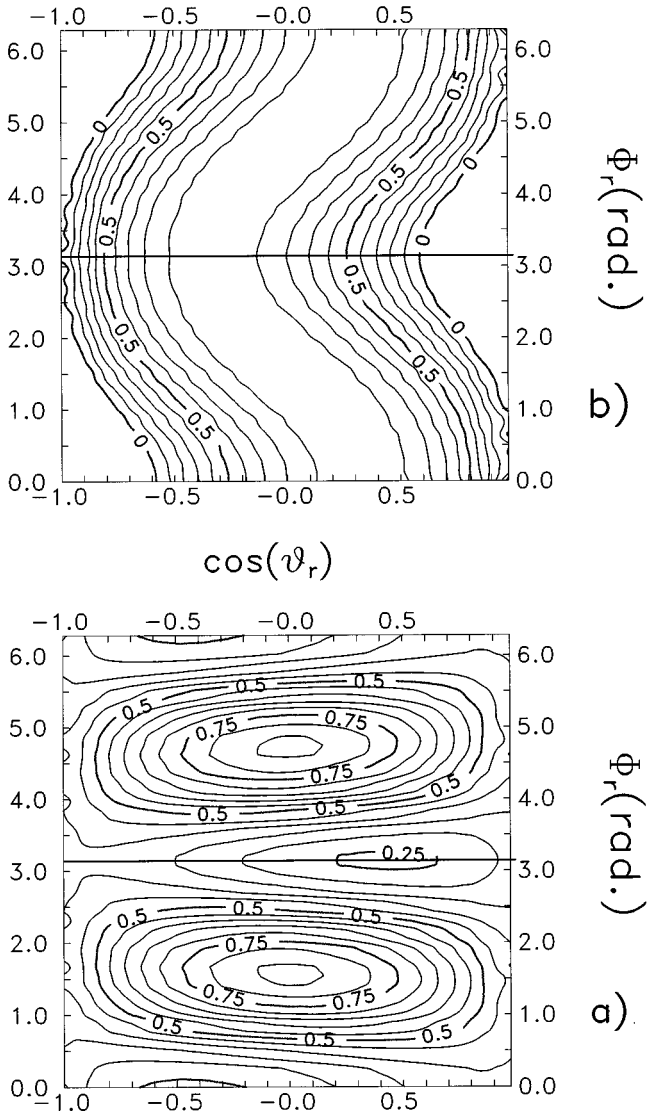

FIG. 9. Polar plots of the $P(\theta_r,\phi_r)$ distribution obtained using only even k moments up to $k=2$, and averaged either over all scattering angles (a), or just over the backward scattering angles $\theta_t=150°$ to 180° (b).

be specialized to a wide variety of experiments including crossed-beam as well as jet-cooled photon-initiated studies of bimolecular reactions.

The 1+1 LIF (or REMPI) Doppler broadened profile of the products of a photon initiated bimolecular reaction may be written[19,21,23]

$$D(v_p)=\int_{v=|v_p|}^{\infty}\frac{1}{2v}\left[\sum_{L=0}^{4} g_L(v)P_L\left(\frac{v_p}{v}\right)\right]dv. \tag{58}$$

v_p is the component of the product LAB velocity along the probe Laser propagation direction and the dominant contributions to the g_L factors may be written[19]

$$g_0(v)=b_0\overline{\beta_0^0(0,0;v)}+b_1\frac{\beta}{2}\overline{\beta_0^2(0,2;v)},$$

$$g_2(v)=b_2\frac{\beta}{2}\overline{\beta_0^2(2,0;v)}+b_3\overline{\beta_0^0(2,2;v)}+b_4\frac{\beta}{2}\overline{\beta_0^2(2,2;v)}, \tag{59}$$

$$g_4(v)=b_6\frac{\beta}{2}\overline{\beta_0^2(4,2;v)},$$

where $\overline{\beta_0^K(k_1,k_2;v)}$ are the rescaled bipolar moments defined in Eqs. (38), (43), (51), and (54) and Tables I and II. The angular momentum coupling and geometrical factors, b_i, defined previously,[19,21] depend on pump–probe geometry and rotational branch, and thus sums of Doppler profiles (*composite Doppler profiles*[19,34]) may be constructed which project out different bipolar moment terms in Eqs. (58) and (59). These composite profiles may be written, approximately

$$D_0^K(k_1,k_2;v_p)=\int_{v=|v_p|}^{\infty}\frac{1}{2v}\overline{\beta_0^K(k_1,k_2;v)}P_{k_1}\left(\frac{v_p}{v}\right)dv \tag{60}$$

and are simulated in the following sections: the details of their construction from experimental data have been presented previously.[19,34] In practice, experimentally obtained composite profiles may depend on more than one of the bipolar moment terms given above. In particular, explicit account should be taken, when simulating experimental composite profiles, of the bipolar moment $\overline{\beta_0^2(4,2;v)}$, which contributes to the P_4 term in Eq. (58). This moment is not readily isolated from the lower order bipolar moments by constructing composite profiles, and is particularly important in composite geometries IIb and IIIb defined in Ref. 17. Fortunately, $\overline{\beta_0^2(4,2;v)}$ depends on the same polarization dependent differential cross-sections as $\overline{\beta_0^2(0,2;v)}$, $\overline{\beta_0^0(2,2;v)}$ and $\overline{\beta_0^2(2,2;v)}$ (see Tables I and II), so the effect this bipolar moment has on the simulated experimental composite profiles is accounted for easily. The remaining four moments not explicitly included in Eqs. (58) and (59), but identified in Refs. 21 and 34, have sufficiently small premultipliers, b_i, to be neglected in the simulation of the composite profiles.

We first compare simulated composite Doppler profiles using the approximate 1-D and full 3-D integrations over the precursor and reagent thermal motions, with a view to illustrating the differences between the two procedures. These simulations employ delta functions for two of the polarization dependent differential cross-sections, corresponding to extreme backward ($\cos\theta_t=-0.95$) and forward ($\cos\theta_t=+0.95$) scattering, i.e.,

$$\frac{1}{\sigma}\frac{d\sigma_{00}}{d\omega_t}=\delta(\cos\theta_t+0.95)\ \text{ or }\ \delta(\cos\theta_t-0.95),$$
$$\frac{1}{\sigma}\frac{d\sigma_{20}}{d\omega_t}=\delta(\cos\theta_t+0.95)\ \text{ or }\ \delta(\cos\theta_t-0.95). \tag{61}$$

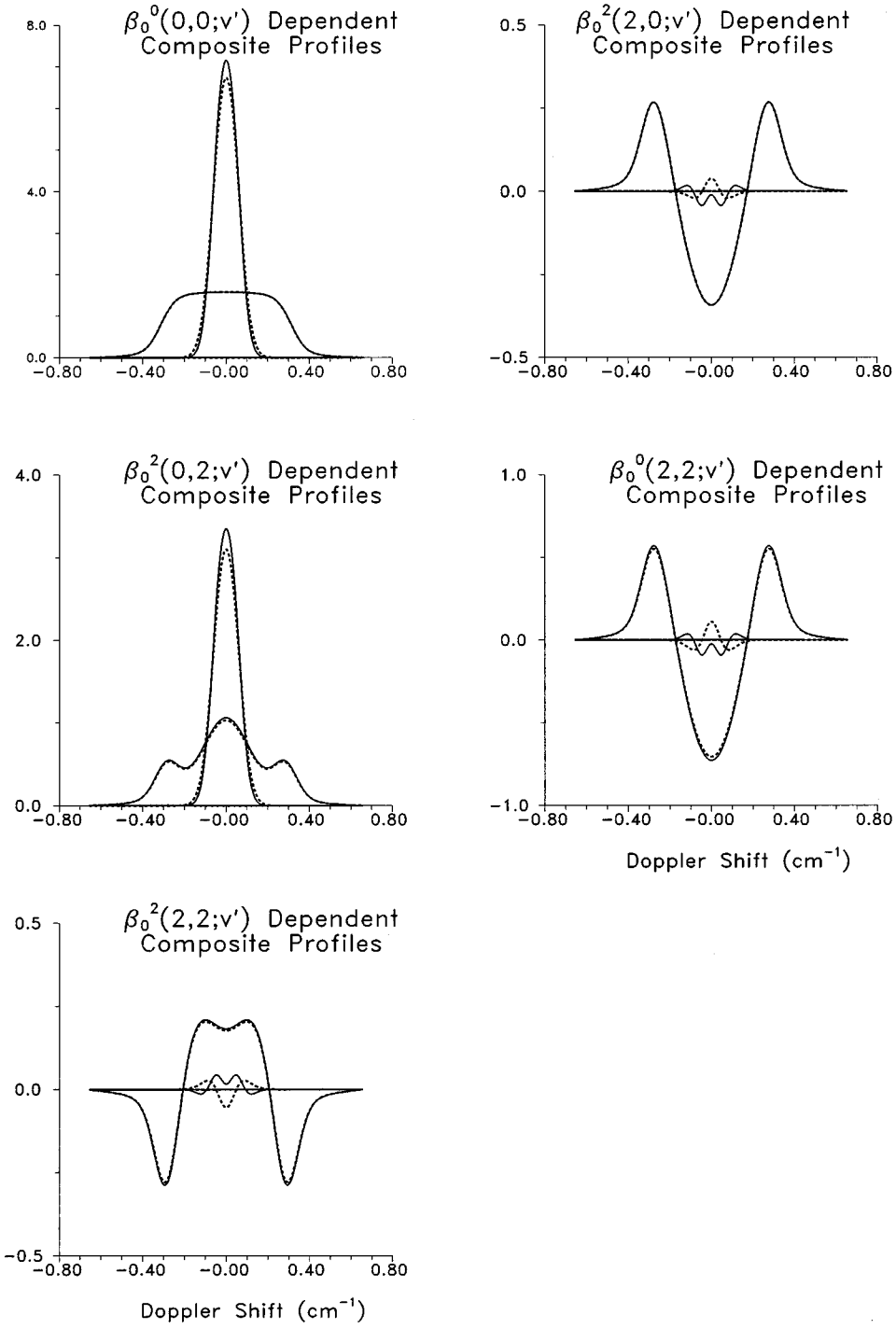

FIG. 10. Comparison of composite Doppler profiles corresponding to extreme forward (wide profiles) and backward (narrow profiles) scattering obtained employing the full 3-D integration (dashed line) with those obtained using the 1-D integration (solid line) over the reagent velocities. The dominant contribution to the composite profiles is given in each panel, but the lower three figures also include the effects of the $\beta_0^2(4,2;v)$ term, which in practice is difficult to separate from the lower moments in the commonly employed pump–probe geometries (see the text for details).

This choice of distribution function is the same as would be employed to generate Doppler profile ''basis functions'' to fit experimental polarization data, as described in Refs. 18 and 23. The remaining polarization dependent differential cross-sections are set equal to zero, but the effects illustrated below are mirrored for all of the polarization dependent differential cross-sections. The simulations employ the kinematics of the $O(^1D)+CH_4 \rightarrow OH+CH_3$ reaction, with an $O(^1D)$ speed distribution and translational anisotropy ($\beta=0.48$) appropriate for the photolysis of N_2O at 193 nm.[9,17] Thermal (300 K) motion of the precursor molecule is accounted for in both the 1-D and 3-D calculations. The CH_3 fragment is treated as a pseudoatom which soaks up a fixed internal energy such that kinetic energy is conserved, as is found to be the case, on average, experimentally.[39] Finally, the simulated composite profiles have been convoluted with

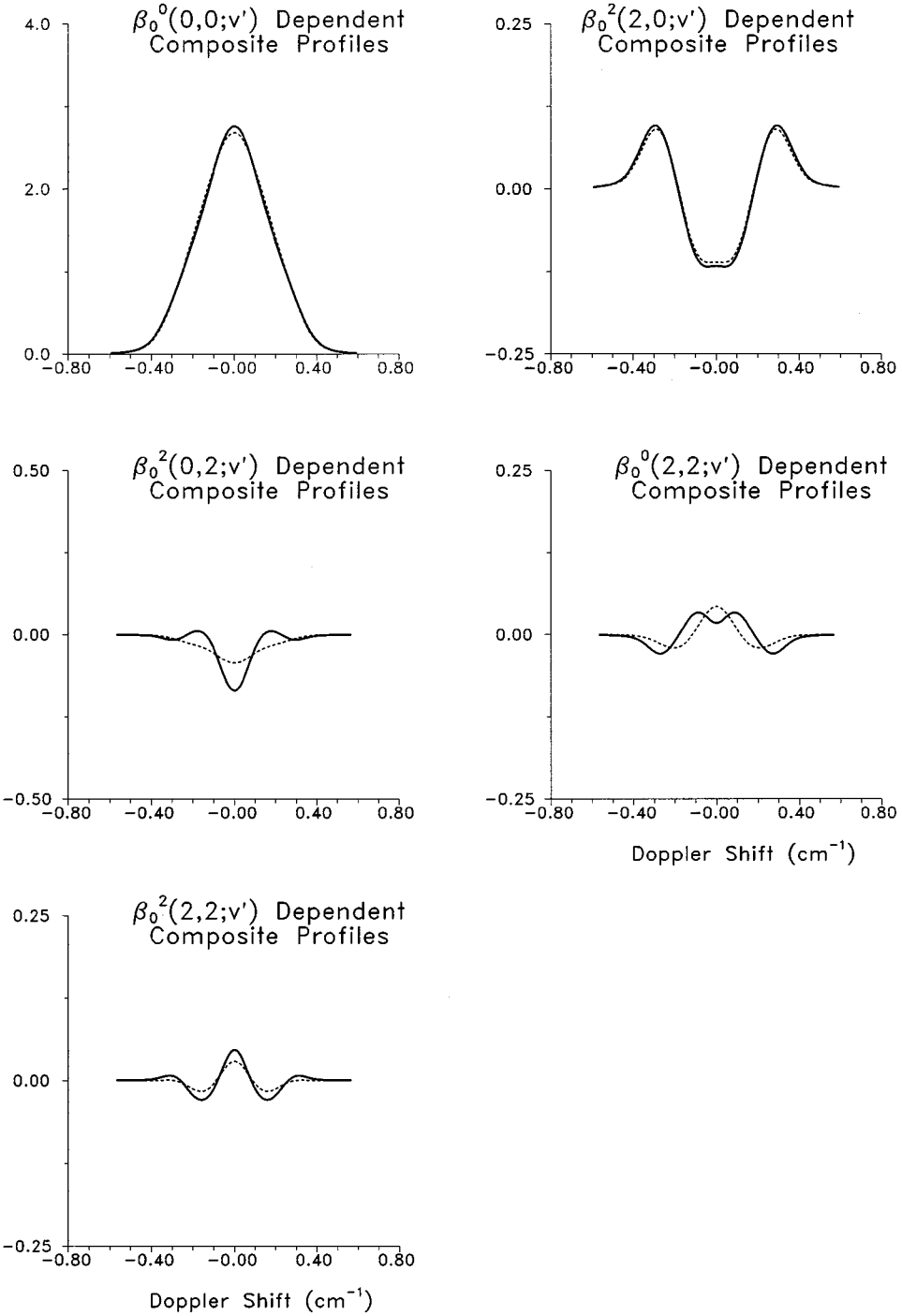

FIG. 11. As for Fig. 10 but showing the LAB frame composite Doppler profiles obtained using the $k=0$ and 2 PDDCS obtained in Sec. IV A 2. The solid line is the simulated profile using all the $s^{k_1}_{kq\pm}$ coefficients up to $k=7$, whilst the dashed line employs only the first $s^{k_1}_{kq\pm}$ moment of the PDDCS (see the text for details). All simulations employ the full 3-D integration over reagent velocities.

a laser Gaussian lineshape function of 0.08 cm^{-1} full-width-half-maximum. Further details of the procedures employed in generating these ''basis functions,'' as well as those required for taking proper account of the internal energy distribution in reactions involving polyatomic co-fragments can be found in Refs. 18, 23, and 39.

Figure 10 summarizes the results of the simulations, and illustrates some general points. First, it is found that composite profiles corresponding to extreme forward scattering (the wide profiles) are very well approximated by 1-D integration. This observation is to be expected since forward scattering in the CM frame corresponds to scattering closer to the vector $\mathbf{v}_1$ in the LAB frame, thus minimizing the effects of a thermal distribution of target reagent molecular velocities, $\mathbf{v}_2$. Conversely, for backward scattering, which corresponds to LAB frame scattering towards $\mathbf{v}_2$, the effect of the neglect of integration of the target molecule motion over angular coordinates is more apparent. The low anisotropies

associated with backward scattering in some of these simulations primarily reflect the kinematics and energetics of the chosen reaction, which are such that for backward scattering $v = v_{cm} - w \sim 0$, where the anisotropy must approach zero.

For the system chosen, the $O(^1D)$ velocity has an average value of 3000 ms^{-1}, which is about five times that of the target methane molecule. In cases where the target molecule thermal motion is a larger fraction of the velocity of the photolytically generated reagent then the differences between 1-D and 3-D integration will tend to be more apparent. In any event, full 3-D integration will probably be necessary when the product LAB velocity, v, approaches the average thermal velocity of the target molecule. For average LAB velocities greater than this, however, the 1-D treatment of the composite profiles, which can be computed about an order of magnitude faster than in the 3-D case, is probably sufficient, at least for preliminary modeling or fitting of experimental data.

Simulated experimental composite profiles, generated using the QCT calculated PDDCS of the preceeding section, are shown in Fig. 11. Since each of the CM generalized differential cross-sections obtained from the calculations is expressed in terms of the $s^{k_1}_{kq\pm}$ coefficients of the modified spherical harmonic expansion given in Eqs. (10) and (13), simulation of the LAB frame moments and composite profiles is most conveniently achieved using a ''contracted basis function'' strategy described in Refs. 17, 18, 23, and 39. The simulations employ the kinematics and energetics of the $O(^1D)+CH_4$ reaction, as described above. The LAB frame anisotropies, upon which the data shown in Fig. 11 depend, are calculated to be rather small, reflecting the small magnitudes of the CM PDDCS employed in the simulations. However, the composite profiles are sufficiently intense to be detectable using the currently available technology, and in fact are of similar magnitude to those observed experimentally for the $O(^1D)+CH_4$ reaction.[17] Also shown in Fig. 11 (as dashed lines), are the composite profiles that would be observed if the PDDCS depended on only the first moments of the expansion given in Eqs. (10) and (13). The profiles which depend solely on the differential $(\mathbf{k},\mathbf{k}')$ cross-section (those at the top of the figure) are little altered by ignoring higher moments of the CM scattering angle distribution, simply reflecting the fact that this distribution is dominated by the first moment, and is nearly isotropic. In contrast, the profiles which are sensitive to the PDDCS with $k \neq 0$ show significant changes when higher moments are ignored. It is these higher moments which are required to characterize the CM scattering angle dependence of the PDDCS, and it is encouraging to note that, for this system at least, the LAB frame composite profiles are sensitive to this dependence.

V. SUMMARY AND CONCLUSIONS

A semiclassical formalism is presented, based on a bipolar moment expansion methodology, for the characterization of the rotational polarization of the products of bimolecular reactions. Equations relating the moments of the bipolar harmonic expansion to the polarization dependent differential cross-sections introduced by Shafer-Ray *et al.*[21] are provided, which facilitate the calculation of the CM PDDCS using QCT techniques. Expressions are given relating the CM PDDCS to the LAB frame bipolar moments obtainable either from studies in cross-molecular beams or of photon-initiated bimolecular reactions, including explicit equations for the LAB moments which can be measured experimentally using 1+1 Doppler-resolved linearly polarized laser detection methods. The resulting machinery is illustrated via QCT calculation of PDDCS and correlated $\mathbf{k},\mathbf{k}',\mathbf{j}'$ angular distributions for the $O(^1D)+HD$ reaction. The calculated PDDCS have also been employed in numerical simulations of the LAB frame bipolar moments and Doppler-resolved profiles most readily measured experimentally. For the insertion reactions under consideration, the resulting composite Doppler profiles are shown to be sensitive to the scattering angle dependence of the polarization dependent differential cross-sections.

ACKNOWLEDGMENTS

We gratefully acknowledge N. E. Shafer-Ray for providing us with a copy of Ref. 21 prior to its publication and also the British Council and Spanish Ministry of Education for the award of a grant under the *Acciones Integradas* programme. We are also indebted to Vicente Sáez-Rábanos for helpful discussions regarding Euler angles. F.J.A. acknowledges the Spanish Ministry of Education for a Fellowship on *Programma de Movilidad temporal de Investigadores y Professors de Universidad*, which allowed for an extended stay at the PTCL in Oxford, and for the grant from the DG1CYT (PB92-0219-C03). Finally, P.A.E. also thanks the Spanish Ministry of Education for the grant from the DGCYT (PB92-0756).

APPENDIX: EULER ANGLES

In the v_1 frame the unit vector in the direction of $\mathbf{k} \neq \hat{\mathbf{k}}$, lies in the XZ plane, and it forms an angle θ_k with the Z axis, so the component of $\hat{\mathbf{k}}$ in that direction has the v_1 frame cartesian coordinates $r_F = (-\sin\theta_k, 0, \cos\theta_k)$. Since $\hat{\mathbf{k}}$ was chosen as the z-axis in the CM scattering frame, its Cartesian coordinates in that frame are $r_g = (0,0,1)$. In addition, the v_1 frame XZ plane forms an angle ϕ_t with the CM frame xz plane (this angle is defined explicitly in Fig. 3). So the cartesian coordinates in the v_1 frame of the unit vector along the CM x axis are $r_F = (\cos\theta_k \cos\phi_t, \sin\phi_t, \sin\theta_k \cos\phi_t)$.

Both sets of coordinates are related by a unitary transformation

$$r_F = \mathscr{R}(\alpha,\beta,\gamma)^{-1} r_g, \tag{A1}$$

where α, β, and γ correspond to the Euler angles of the coordinate transformation as defined by Messiah,[30] and $\mathscr{R}(\alpha,\beta,\gamma)^{-1}$ represents the inverse of the direction cosine rotation matrix defined by Messiah[30] Eq. C.45. Note that the transformation given by Eq. (A1) carries the CM scattering frame to the v_1 frame and that, apart from the definition of the angle ϕ_t, we employ the Messiah convention throughout. The angle ϕ_t is defined here as the dihedral angle which

takes the v_1 XZ plane to the CM xz plane, as shown in Fig. 3. Written explicitly in terms of the direction cosines, the transformation [Eq. (A1)] reads, for the CM z-axis

$$\begin{pmatrix} -\sin\theta_k \\ 0 \\ \cos\theta_k \end{pmatrix} = \begin{pmatrix} c\alpha c\beta c\gamma - s\alpha s\gamma & s\alpha c\beta c\gamma + c\alpha s\gamma & -s\beta c\gamma \\ -c\alpha c\beta s\gamma - s\alpha c\gamma & -s\alpha c\beta s\gamma + c\alpha c\gamma & s\beta s\gamma \\ c\alpha s\beta & s\alpha s\beta & c\beta \end{pmatrix} \times \begin{pmatrix} 0 \\ 0 \\ 1 \end{pmatrix}, \tag{A2}$$

where c and s represents cos and sin, respectively. Equation (A2) yields the following equations:

$$\left.\begin{aligned} -\sin\theta_k &= -\sin\beta\cos\gamma \\ 0 &= \sin\beta\sin\gamma \\ \cos\theta_k &= \cos\beta \end{aligned}\right\} \Rightarrow \begin{matrix} \beta=\theta_k, & \gamma=0 \\ \beta=-\theta_k, & \gamma=\pi. \end{matrix} \tag{A3}$$

In the case of the CM x axis, with the Euler angles $\beta=\theta_k$ and $\gamma=0$, the transformation is given by

$$\begin{pmatrix} \cos\theta_k\cos\phi_t \\ \sin\phi_t \\ \sin\theta_k\cos\phi_t \end{pmatrix} = \begin{pmatrix} c\theta_k c\alpha & c\theta_k s\alpha & -s\theta_k \\ -s\alpha & c\alpha & 0 \\ s\theta_k c\alpha & s\theta_k s\alpha & c\theta_k \end{pmatrix} \begin{pmatrix} 1 \\ 0 \\ 0 \end{pmatrix}, \tag{A4}$$

which implies that $\alpha=-\phi_t$. For the Euler angles, $\beta=-\theta_k$ and $\gamma=\pi$, it is easily shown that $\alpha=\pi-\phi_t$. Thus the Euler angles that define the transformation from the CM to the frame v_1 scattering frame are

$$\alpha=-\phi_t, \quad \beta=\theta_k, \quad \gamma=0$$

or

$$\alpha=\pi-\phi_t, \beta=-\theta_k, \quad \gamma=\pi.$$

Thus the CM frame $\mathbf{k}-\mathbf{k}'-\mathbf{j}'$ distribution

$$P(\omega_t,\omega_r)=\sum_{kq}\frac{[k]}{4\pi}\frac{1}{\sigma}\frac{d\sigma_{kq}}{d\omega_t}C_{kq}(\theta_r,\phi_r)^* \tag{A6}$$

can be related to the $\mathbf{v}_1-\mathbf{v}-\mathbf{j}'$ distribution function, $P(\omega_v,\omega_j)$, by[19,30]

$$\begin{aligned} P(\omega_v,\omega_j;v) &= \sum_{kq}\frac{[k]}{4\pi}\sum_{q'} D^k_{q'q}(-\phi_t,\theta_k,0)\frac{1}{\sigma}\frac{d\sigma_{kq'}}{d\omega_t} \\ &\quad\times C_{kq}(\theta_j,\phi_j)^*\frac{v^2}{w_i^2}\delta(w-w_i) \\ &= \sum_{kq}\frac{[k]}{4\pi}\sum_{q'} D^k_{q'q}(-\phi_t,\theta_k,0) \\ &\quad\times\frac{1}{\sigma}\frac{d\sigma_{kq'}}{d\omega_t}C_{kq}(\theta_j,\phi_j)^* \\ &\quad\times\delta(\cos\theta_v-\cos\theta_v^i)\left|\frac{d\cos\theta_v}{dw_i}\right|\frac{v^2}{w_i^2}. \end{aligned}$$

Notice that in these expressions the rotation matrices are defined as[30]

$$D^k_{q'q}(\alpha,\beta,\gamma)=e^{-iq'\alpha}d^k_{q'q}(\beta)e^{-iq\gamma}.$$

[1] U. Fano and J. H. Macek, Rev. Mod. Phys. **45**, 553 (1973).
[2] D. E. Case and D. R. Herschbach, Mol. Phys. **30**, 1537 (1975).
[3] G. M. McClelland and D. R. Herschbach, J. Phys. Chem. **83**, 1445 (1979).
[4] J. D. Barnwell, J. G. Loeser, and D. R. Herschbach, J. Phys. Chem. **87**, 2781 (1983).
[5] Throughout the paper, ω_t refers to the polar coordinates of the product velocity, w', in the centre-of-mass frame. We also note at the outset that a simplified notation will be employed: $d\sigma/d\omega_t$ is written as a short-hand for the double differential cross-section $d^2\sigma/d^2\omega_t$.
[6] A. J. Orr-Ewing and R. N. Zare, Ann. Rev. Phys. Chem. **45**, 315 (1994).
[7] A. J. Orr-Ewing and R. N. Zare, in *Chemical Dynamics and Kinetics of Small Radicals*, edited by A. Wagner and K. Liu (World Scientific, Singapore, 1995).
[8] M. Brouard and J. P. Simons, in *Chemical Dynamics and Kinetics of Small Radicals*, edited by A. Wagner and K. Liu (World Scientific, Singapore, 1995).
[9] M. Brouard, S. Duxon, and J. P. Simons, J. Chem. Phys. **97**, 7414 (1992).
[10] H. L. Kim, M. A. Wickramaaratchi, and G. E. Hall, J. Chem. Phys. **101**, 2033 (1994).
[11] D. F. Varley and P. J. Dagdigian, J. Phys. Chem. **99**, 9843 (1995).
[12] W. R. Simpson, A. J. Orr-Ewing, and R. N. Zare, Chem. Phys. Lett. **212**, 163 (1993).
[13] W. R. Simpson, A. J. Orr-Ewing, S. A. Kandel, T. P. Rakitzis, and R. N. Zare, J. Chem. Phys. **103**, 7299 (1995).
[14] W. R. Simpson, T. P. Rakitzis, S. A. Kandel, A. J. Orr-Ewing, and R. N. Zare, J. Chem. Phys. **103**, 7313 (1995).
[15] W. R. Simpson, T. P. Rakitzis, S. A. Kandel, Topaz Lev-On, and R. N. Zare, J. Phys. Chem. **100**, 7938 (1996).
[16] M. Brouard, S. Duxon, P. A. Enriquez, and J. P. Simons, J. Chem. Soc. Faraday Trans. **89**, 1432 (1993).
[17] M. Brouard, H. M. Lambert, J. Short, and J. P. Simons, J. Phys. Chem. **99**, 13571 (1995).
[18] M. Brouard, S. P. Rayner, and J. P. Simons, Mol. Phys. (in press).
[19] J. Aoiz, M. Brouard, P. A. Enriquez, and R. Sayos, J. Chem. Soc. Faraday Trans. **89**, 1427 (1993).
[20] N. E. Shafer, A. J. Orr-Ewing, W. R. Simpson, H. Xu, and R. N. Zare, Chem. Phys. Lett. **212**, 155 (1993).
[21] N. E. Shafer, A. J. Orr-Ewing, and R. N. Zare, J. Phys. Chem. **99**, 7591 (1995).
[22] R. N. Dixon, J. Chem. Phys. **85**, 1866 (1986).
[23] F. J. Aoiz, M. Brouard, and H. M. Lambert (in preparation).
[24] D. M. Brink and G. R. Satchler, *Angular Momentum*, 3rd ed. (Oxford University Press, Oxford, 1993).
[25] R. N. Zare, *Angular Momentum, Understanding Spatial Aspects in Chemistry and Physics* (Wiley, New York, 1988).
[26] L. C. Biederharn, *Nuclear Spectroscopy, Part B*, edited by F. Azjenber-Selove (Academic, New York, 1960), p. 732.
[27] K. Blum, *Progress in Atomic Spectroscopy, Part A*, edited by W. Hanle

and K. Kleinpoppen (Plenum, New York, 1978), p. 95.
[28] We employ here a simplified notation: $b_Q^K(k_1,k_2;v) \equiv b_Q^K(k_1,k_2;v,v_1,v_2)$.
[29] C. H. Greene and R. N. Zare, J. Chem. Phys. **78**, 6741 (1983).
[30] A. Messiah, *Quantum Mechanics* (North Holland, Amsterdam, 1975).
[31] We also employ here a simplified notation: $b_Q^K(k_1,k_2;v) \equiv b_Q^K(k_1,k_2;v,\mathbf{v}_1,\mathbf{v}_2)$.
[32] A. J. Alexander, F. J. Aoiz, M. Brouard, and J. P. Simons, Chem. Phys. Lett. **256**, 561 (1996).
[33] A. J. Alexander, F. J. Aoiz, and M. Brouard (in preparation).
[34] M. P. Docker, Chem. Phys. **135**, 405 (1989).
[35] R. Schinke and W. A. Lester, J. Chem. Phys. **72**, 3754 (1980).
[36] F. J. Aoiz, V. J. Herrero, and V. Sáez-Rabanos, J. Chem. Phys. **97**, 7423 (1992).
[37] T. Peng, D. H. Zhang, J. Z. H. Zang, and R. Schinke, Chem. Phys. Lett. **248**, 37 (1996).
[38] S. K. Kim and D. R. Herschbach, Faraday Discuss. Chem. Soc. **84**, 159 (1987).
[39] M. Brouard, H. M. Lambert, C. L. Russell, J. Short, and J. P. Simons, Faraday Discuss. **102** (in press).